Pre-Print of Mechanics of Advanced Materials and Structures 2023
https://doi.org/10.1080/15376494.2023.2277849

Orthotropic Damage Model for Composite Structures using the 3D Tsai-Wu Failure Criterion

M.R.T. Arruda

Research Associate, CERIS, Instituto Superior Técnico, Universidade de Lisboa, Portugal
(mario.rui.arruda@tecnico.ulisboa.pt)

Abstract: This paper presents a novel approach concerning the development of an orthotropic damage model based on the original 3D Tsai-Wu failure criterion. In its original formulation, the Tsai-Wu criterion is only capable of identifying the existence of damage at a certain point in the material. However, it is not capable of identifying if the damage is located in the fiber, matrix or interlaminar zone. This work plans to fill this gap in knowledge by providing a simple method, based on equivalent stresses and strains, that identifies the failure modes when the Tsai-Wu failure criterion is near the on-set of damage. Using this novel method, it is possible to implement classical damage evolution laws based on the formulation of Matzenmiller. The proposed damage model is implemented in the commercial finite element software ABAQUS using user-subroutine UMAT, and the numerical results are compared with experimental data obtained earlier by other authors for different applications of glass fibre reinforced polymer (GFRP) structures. The numerical stabilization is achieved by using a new implicit to explicit material time step algorithm.

Keywords: Tsai-Wu Criterion, 3D Orthotropic Damage Model, Energy Regularization, Stabilization Algorithm, Composite Structures

1 Introduction

The development of new three-dimensional (3D) orthotropic damage models for fibre-polymer composite materials is mainly associated with the need to incorporate them in solid finite element models in order to accurately simulate problems where stress concentrations and multi-axial stresses (including in-plane and out-of-plane stresses) are relevant, such as the mechanical behaviour of three-dimensional connections [El Kadi et al. 2022; Li et al. 2021; Martins et al. 2017]. In some cases, several two-dimensional (2D) orthotropic damage models have been used in conjunction with shell-elements to simulate the behaviour of exterior profiles in hybrid beams and new carbon fiber reinforced aluminium laminates [Hu et al. 2022; Kong et al. 2020]. However, other authors found limitations in using classical 2D formulation with continuum shell elements to numerically simulate glass-fibre reinforced polymer (GFRP) connections [Girão Coelho et al. 2015], related to accuracy in simulating either pilling, shear-out, or bearing failure due to the incorrect stress distribution in the thickness obtained when using shell formulation for non-linear analysis. Due to the rapid proliferation of composite structures in different industries [Correia et al. 2015], the need for a wider 3D orthotropic damage formulation has been pursued since the beginning of 2000s [Carol et al. 2002]. The accuracy of the computed stress level depends on the problem being analysed at the micro, meso, or macro scale [Arteiro et al. 2019], which in all cases must always be formulated in 3D. The application of a full 3D orthotropic damage model still presents some challenges for the structural designer, such as a: full 3D formulation with explicit material parameters; simple and clear guidelines for direct application. These two aspects are fundamental for the structural designer since, in the scientific community, these orthotropic damage models are basically used to validate experimental campaign and adopted material properties [Chowdhury et al. 2021; Granados et al. 2021]. Unfortunately, the use of

composite orthotropic damage models by academic researchers are not being used without an existing experimental campaign to achieve better design solutions, and this is an engineering fundamental need in the industry of composites due to the lack of structural codes for these materials.

1.1 Objectives

This work has two fundamental objectives. The first is to study the numerical efficiency of a new 3D orthotropic damage model based on the Tsai-Wu failure criterion, using classical MTL damage progression [Matzenmiller et al. 1995] with energy regularization [Lopes et al. 2020]. This orthotropic damage model is compared and validated with experimental data. The second objective is to compare and improve the 3D Hashin damage model previously proposed in [Arruda et al. 2023], which is a standard in the scientific community, and compare it with the proposed Tsai-Wu based damage model.

1.2 Research Significance

The novelty of this research is the proposal of a full 3D orthotropic damage model, based on the Tsai-Wu failure criterion, using the combination of damage evolution with fracture energy regularization and residual stresses, which allows the simulation of complex collapse modes, like the transition from bearing to shear out in composite bolt connections. According to the authors' best knowledge, this has never been done, and this present paper aims at filling this gap in knowledge.

2 Recent Advances in 3D Orthotropic Damage Models

Since the 2000s, several 3D orthotropic damage models have been proposed. This is mainly due to the popularity in the scientific community of commercial finite element software in implementing new material constitutive relations [ABAQUS 2018; ANSYS 2015].

Before the mass proliferation of 3D orthotropic damage models, simple 2D orthotropic damage models were used for shell elements due to the composite ply-by-ply behaviour and simplification in the formulation [Lapczyk et al. 2007]. These 2D orthotropic damage models were sufficient to simulate beams [Kong et al. 2020], columns [Kang et al. 2021] and composite sandwich panels [Arruda et al. 2018], but with severe limitations when simulating 3D beam-to-column connections [Girão Coelho et al. 2015].

The difficulty in evolving from a 2D to a 3D failure model is mainly to the first being assembled and tested using plane analysis [Chen et al. 2019; Nahas 1986]. This leads to different results when a formulation is then extended in the 3rd dimension [Kaddour et al. 2013]. In addition, the 3D failure criterion and damage evolution may depend severely on the type of orthotropic composite material being studied. The use of the 3D Hashin failure criterion is not new and has been proposed for shell elements [Hashin 1981] and for solid elements [Camanho et al. 1999; Hühne et al. 2010], in any case without any proposal for interlaminar failure. A popular 3D method based on the combination of several elliptic surfaces for the adoption of separated failure criterion [Cheng et al. 2017], presented encouraging results in simulating the connection of 3 bolt joints for T300/5228A composite material with discontinuous damage evolution. Some variations of these elliptic surfaces were used for stochastic analysis of peek laminates [Naderi et al. 2013]. For composite fibre metals, fibre and matrix 3D failure criterion are based on a square root sum of total strains [Linde et al. 2004], but with a cohesive interlaminar failure criterion. A variation of this last method was applied in Fibre Reinforced Polymers (FRP) composites [Liu et al. 2014; Wang et al. 2009], but with limitations to material orientation on the failure criterion. One of the first successful applications in 3D analysis with Larc05 was presented in the work of [Gutkin et al. 2009], with

variations proposed by [Chen et al. 2022; Warren et al. 2016]. 3D failure criterion with simple degradation models [Olmedo et al. 2012] in terms of elastic parameters have also been successful and continue to be popular among structural engineers due to their simplicity of implementation. One of the most successful applications of a fully 3D Hashin failure criterion with simple degradation models was proposed by [Mandal et al. 2017], for bolted connections and to inquire about fracture energy levels [Arruda et al. 2023]. In recent times, the Hou criterion, based on an enhanced 3D elliptic failure surface [Wang et al. 2018], used explicit formulations to simulate drilling damage. To improve the matrix damage evolution due to higher shear, the NU (North-western University) failure criterion was proposed and applied in a three-point bending load [Liu et al. 2020]. Recently, the use of invariant base formulation started to produce great results concerning the bearing in composite connections [Camanho et al. 2015; Zhuang et al. 2019]. It is important to point out, that even though these new 3D orthotropic damage models, possess a robust formulation, most of them suffer from having too many input material parameters that are very difficult to obtain in experimental campaigns, in which alternative methodologies for estimating them are needed [Zhan et al. 2023].

3 3D Orthotropic Stiffness Formulation

To ease the orthotropic formulation description in the UMAT subroutine, ABAQUS standard notation is used for both stress and strain tensors [Barbero 2013]. The elastic constitutive relation for the stress σ_i and strain ε_i are based on the compliance H_{ij}^d and stiffness matrix C_{ij}^d respectively (1).

$$\varepsilon_i = H_{ij}^d \sigma_j \quad [H_d]^{-1} = [C_d] \quad \sigma_i = C_{ij}^d \varepsilon_j \tag{1}$$

with:

$$\begin{gathered}\sigma_1 = \sigma_{11}; \sigma_2 = \sigma_{22}; \sigma_3 = \sigma_{33}; \sigma_4 = \tau_{12}; \sigma_5 = \tau_{13}; \sigma_6 = \tau_{23} \\ \varepsilon_1 = \varepsilon_{11}; \varepsilon_2 = \varepsilon_{22}; \varepsilon_3 = \varepsilon_{33}; \varepsilon_4 = \gamma_{12}; \varepsilon_5 = \gamma_{13}; \varepsilon_6 = \gamma_{23}\end{gathered} \tag{2}$$

Just like in the previous 2D Hashin formulation [Lapczyk et al. 2007], the tension and compression damage (d_t, d_c) are activated using the respective effective stress space $\hat{\sigma}_i$ (3). For this work, damage variables are related to the fibre d_f, the matrix d_m and the interlaminar d_i, in which they will be separated into their tensile d_t and compressive part d_c. Contrary to what was previously proposed in [Arruda et al. 2021], both Hashin and Tsai-Wu will possess the same orthotropic damage evolution.

$$\hat{\sigma}_i = \frac{\sigma_i}{(1 - d_i)} \tag{3}$$

where:

$$d_1 = d_f; d_2 = d_m; d_3 = d_i; d_4 = d_{s12}; d_5 = d_{s13}; d_6 = d_{s23}$$

For the Hashin criterion:

$$d_f = \begin{cases} d_{ft} & if \quad \hat{\sigma}_1 \geq 0 \\ d_{fc} & if \quad \hat{\sigma}_1 < 0 \end{cases} \tag{4}$$

$$d_m = \begin{cases} d_{mt} & if \quad \hat{\sigma}_2 + \hat{\sigma}_3 \geq 0 \\ d_{mc} & if \quad \hat{\sigma}_2 + \hat{\sigma}_3 < 0 \end{cases} \tag{5}$$

$$d_i = \begin{cases} d_{it} & if \quad \hat{\sigma}_3 \geq 0 \\ d_{ic} & if \quad \hat{\sigma}_3 < 0 \end{cases} \tag{6}$$

For the Tsai-Wu criterion:

$$\begin{cases} d_f = 1 - (1 - d_{ft})(1 - d_{fc}) \\ d_m = 1 - (1 - d_{mt})(1 - d_{mc}) \\ d_i = 1 - (1 - d_{it})(1 - d_{ic}) \end{cases} \tag{7}$$

Regarding the shear damage evolution, it is used the same formulation for both the Hashin and Tsai-Wu damage models. However, for the Tsai-Wu damage model, the shear damage, uses the full value of the damage state (9), instead of the combination of the tensile and compressive in the shear damage (8), like the one classically used in Hashin damage formulation.

For the Hashin criterion:

$$\begin{cases} d_{s12} = 1 - (1 - d_{ft})(1 - d_{fc})(1 - d_{mt})(1 - d_{mc}) \\ d_{s13} = 1 - (1 - d_{ft})(1 - d_{fc})(1 - d_{it})(1 - d_{ic}) \\ d_{s23} = 1 - (1 - d_{mt})(1 - d_{mc})(1 - d_{it})(1 - d_{ic}) \end{cases} \tag{8}$$

For the Tsai-Wu criterion:

$$\begin{cases} d_{s12} = 1 - (1 - d_f)(1 - d_m) \\ d_{s13} = 1 - (1 - d_f)(1 - d_i) \\ d_{s23} = 1 - (1 - d_m)(1 - d_i) \end{cases} \tag{9}$$

To present a coherent and thermodynamically admissible 3D orthotropic stiffness, it is necessary to assemble the damage compliance matrix H_d, using exclusively the diagonal term (10) to take into account the damage behaviour [Dhari et al. 2021; Melro 2011; Warren et al. 2016]. It is then possible to assemble the damaged stiffness matrix C_d, by inverting the previous compliance matrix (12). It is important to state the relevance of Γ_d, since this term guarantees that when subjected to uniform longitudinal stress, no transversal stress occurs. The main advantage is that this matrix, by design, verifies the thermodynamic admissibility principals when using Gibbs free energy [Lemaitre 1992; Lemaitre et al. 2002].

$$[H_d] = \begin{bmatrix} \frac{H_{11}}{1-d_f} & H_{12} & H_{13} & 0 & 0 & 0 \\ H_{21} & \frac{H_{22}}{1-d_m} & H_{23} & 0 & 0 & 0 \\ H_{31} & H_{32} & \frac{H_{33}}{1-d_i} & 0 & 0 & 0 \\ 0 & 0 & 0 & \frac{H_{44}}{1-d_{s12}} & 0 & 0 \\ 0 & 0 & 0 & 0 & \frac{H_{55}}{1-d_{s13}} & 0 \\ 0 & 0 & 0 & 0 & 0 & \frac{H_{66}}{1-d_{s23}} \end{bmatrix} \tag{10}$$

with:

$$\begin{cases} H_{11} = \frac{1}{E_1} \\ H_{22} = \frac{1}{E_2} \\ H_{33} = \frac{1}{E_3} \end{cases} \quad \begin{cases} H_{12} = H_{21} = -\frac{\nu_{12}}{E_1} \\ H_{13} = H_{31} = -\frac{\nu_{13}}{E_1} \\ H_{23} = H_{32} = -\frac{\nu_{23}}{E_2} \end{cases} \quad \begin{cases} H_{44} = G_{12} \\ H_{55} = G_{13} \\ H_{66} = G_{23} \end{cases} \tag{11}$$

$$[C_d] = \Gamma_d \begin{bmatrix} C_{11} & C_{12} & C_{13} & 0 & 0 & 0 \\ C_{21} & C_{22} & C_{23} & 0 & 0 & 0 \\ C_{31} & C_{32} & C_{33} & 0 & 0 & 0 \\ 0 & 0 & 0 & C_{44} & 0 & 0 \\ 0 & 0 & 0 & 0 & C_{55} & 0 \\ 0 & 0 & 0 & 0 & 0 & C_{66} \end{bmatrix} \tag{12}$$

with:

$$\begin{cases} C_{11} = (1-d_f)E_1[1-(1-d_m)(1-d_i)\nu_{23}\nu_{32}] \\ C_{22} = (1-d_m)E_2[1-(1-d_f)(1-d_i)\nu_{13}\nu_{31}] \\ C_{33} = (1-d_i)E_3[1-(1-d_f)(1-d_m)\nu_{12}\nu_{21}] \\ C_{12} = C_{21} = (1-d_f)(1-d_m)E_1[\nu_{21}+(1-d_i)\nu_{31}\nu_{23}] \\ C_{13} = C_{31} = (1-d_i)(1-d_m)E_1[\nu_{31}+(1-d_m)\nu_{21}\nu_{32}] \\ C_{23} = C_{32} = (1-d_m)(1-d_i)E_2[\nu_{32}+(1-d_f)\nu_{31}\nu_{12}] \end{cases} \tag{13}$$

$$\begin{cases} C_{44} = (1-d_{s12})G_{12}/\Gamma_d \\ C_{55} = (1-d_{s13})G_{13}/\Gamma_d \\ C_{66} = (1-d_{s23})G_{23}/\Gamma_d \end{cases} \tag{14}$$

$$\begin{cases} \Gamma_d = (1-\Gamma_{fm}\nu_{12}\nu_{21}-\Gamma_{mi}\nu_{23}\nu_{32}-\Gamma_{fi}\nu_{13}\nu_{31}-2\times\Gamma_{fmi}\nu_{12}\nu_{23}\nu_{31})^{-1} \\ \Gamma_{fm} = (1-d_f)(1-d_m) \\ \Gamma_{mi} = (1-d_m)(1-d_i) \\ \Gamma_{fi} = (1-d_f)(1-d_i) \\ \Gamma_{fmi} = (1-d_f)(1-d_m)(1-d_i) \end{cases} \tag{15}$$

All continuum damage models require the definition of an evolution law and must be consistent with the first and second thermodynamic laws [Barbero 2013; Proença 2000].

$$\Psi = \Psi(\sigma, d_i, z_j) = \frac{1}{2}\{\sigma\}^t[C_d]\{\sigma\} \tag{16}$$

To use these constitutive laws, it is necessary to define a thermodynamic potential function, denoted here as Ψ (16). The variables d_i and z_j are used to control the dissipation mechanism of the material, which is not measurable, and are usually defined as internal state variables. The variable z_j (defined below) is used to control the spread of damage in certain directions when effective stresses are not predominant. This is necessary to control the fibre and matrix damage distribution since the Tsai-Wu criterion is only one single failure criterion. For the Hashin criterion the value of z_j is non-existent.

$$\begin{cases} \varepsilon = \dfrac{\partial\Psi}{\partial\sigma} \\ Y_i = \dfrac{\partial\Psi}{\partial d_i} \\ Z_j = \dfrac{\partial\Psi}{\partial z_j} \end{cases} \tag{17}$$

$$Y_i\delta d_i \geq 0 \quad \& \quad Z_j\delta z_j \geq 0 \tag{18}$$

It is possible to define a set of associated variables by deriving the potential Ψ. Conventionally, Y are referred in the scientific community as the thermodynamic forces. It is beyond the scope of this work,

but it can be demonstrated in the work of [Barbero 2013; Proença 2000] that a damage model is thermodynamically admissible [Ziegler 1977] if the thermodynamic forces, defined in (17), fulfil the equation (18).

$$F(\sigma, d, z) \leq 0 \tag{19}$$

To assemble a damage model, it is necessary to define a "loading function" F that may depend on the primary and secondary state variables, as expressed in (19). The most common definition for this function is to use negative values for the elastic domain and a null value when the material can dissipate energy by developing damage.

$$\begin{array}{ccccc} F \leq 0 & \& & \delta d \geq 0 & \& & \delta d.F = 0 \\ & \& & \delta z \geq 0 & \& & \delta z.F = 0 \end{array} \tag{20}$$

It can be demonstrated that when using equations (19) and (20), it is possible to formulate the known loading and unloading Kuhn-Tucker conditions [Lemaitre et al. 2002], as expressed by equations (21). The first two inequalities define the domain of validity of each variable, *i.e.,* the dissipation potential must be non-positive and the damage increments cannot be negative. The third expression relates both variables, imposing that in order to have damage increments, the dissipation potential must be null.

$$\Psi(\sigma, d, z) = \frac{1}{2}\left(\sum_{i=1}^{6} \frac{H_{ii}\sigma_i^2}{1 - d_{i,z}} + \sum_{i,j=1\curvearrowright 2}^{3\curvearrowright 1} 2 \times H_{ij}\sigma_i\sigma_j\right)$$

where:

$$\sigma_1 = \sigma_{11}; \sigma_2 = \sigma_{22}; \sigma_3 = \sigma_{33}; \sigma_4 = \tau_{12}; \sigma_5 = \tau_{13}; \sigma_6 = \tau_{23}$$
$$d_1 = d_f; d_2 = d_m; d_3 = d_i; d_4 = d_{s12}; d_5 = d_{s13}; d_6 = d_{s23} \tag{21}$$

$$d_{i,z} = z_{ij} d_i$$

Since the Hashin and Tsai-Wu failure criterion is written in terms of stresses, the Gibbs energy density defined in equation (21) is used. As defined by [Nguyen 1985], two types of internal state variables are taken into account: the damage, d, and the state direction variable, z, for fibre and matrix in tension and compression. The final damage $d_{i,z}$ is a combination of calculated damage and the state direction variable. This function must be positive definite, and it must be zero at the origin with respect to the free variables.

The thermodynamic forces are defined by equation (22), for the fibre, matrix, interlaminar and shear damage in tension and compression. Since these quantities are always positive, the condition (23) is verified if the damage variable never decreases. This is important since it allows for a simplification of the model.

With the classical orthotropic elastic compliance matrix H_{ii}, when calculating the thermodynamic forces, these are always positive (22), therefore validating the 2nd principal of thermodynamics (23), and demonstrating the damage model is thermodynamically admissible.

With the classical orthotropic elastic compliance matrix H_{ii}, when calculating the thermodynamic forces, these are always positive (22), therefore validating the 2nd principal of thermodynamics (23), and demonstrating the damage model is thermodynamically admissible.

$$Y_i = \frac{\partial \Psi}{\partial d_i} = \frac{1}{2}\frac{H_{ii}\sigma_i^2}{\left(1 - d_{i,z}\right)^2} \geq 0 \tag{22}$$

$$\Rightarrow \sum_i Y_i \delta d_i \geq 0 \tag{23}$$

3.1 3D Hashin based Damage Model

It is important to point out that there is no consensus in the scientific community regarding the true formulation of the 3D Hashin failure criterion. This is due to the fact that the real cross failure criterion between the intralaminar and interlaminar is still highly debatable in the scientific community [Mandal et al. 2017; Naderi et al. 2013]. This uncertainty is still more evident, when the damage evolution laws are studied [Wang et al. 2017; Warren et al. 2016] and several assumptions must be made to fully verify the thermodynamic admissibility criteria.

Contrary to popular belief, the Hashin failure criterion started as a 3D failure criterion to be used in shell elements, and it was later simplified for the 2D plane elements, although they did not possess any interlaminar failure criterion [Hashin 1980; Hashin et al. 1973]. Also, another limitation to this failure model is that it was assembled for unidirectional composites, but many authors still use it for general lamina composites [Barbero et al. 2014; Barbero et al. 2013]. For this work, the initial formulation of the Hashin damage model previously studied in [Arruda et al. 2023] is improved to account for full 3D behaviour during damage evolution.

3.1.1 Hashin 3D Failure Criterion

In this work, the Hashin 3D failure criterion is based on a merging of the formulations proposed by [Camanho et al. 1999], [Hashin 1980] and [Olmedo et al. 2012]. These still admit a main plane behaviour, that is consistence with a principal resistance stress of the material [Girão Coelho et al. 2015], in which its failure criteria are assembled. The original model itself presents some material and tensor field simplifications, since the real behaviour of composites is difficult to represent in the 3D realm. In this work, to extend to a fully 3D behaviour, the Hashin failure criterion presented in [Melro 2011] will be adopted, in which the stresses are written in the effective space domain $\hat{\sigma}_i$, since with damage evolution, the stress may decrease.

The first mode is related to fibre tensile F_{ft} and compressive failure F_{fc} initiation (24), in which X_t and X_c are the fibre tensile and compressive strengths, respectively. This mode is only an extension of the 3D formulation proposed in the work of [Olmedo et al. 2012].

$$\begin{aligned} F_{ft} &= \left(\frac{\hat{\sigma}_1}{X_t}\right)^2 + \frac{\hat{\tau}_{12}^2 + \hat{\tau}_{13}^2}{S_L^2} = 1.0 \qquad if\ \hat{\sigma}_1 \geq 0 \\ F_{fc} &= \left(\frac{\hat{\sigma}_1}{X_c}\right)^2 = 1.0 \qquad if\ \hat{\sigma}_1 < 0 \end{aligned} \tag{24}$$

The second mode is the matrix tensile F_{mt} and compressive F_{mc} failure criterion (25), that depends on the effective stress in the 2-2 and 3-3 axes. Y_t and Y_c are the matrix tensile and compressive strengths, respectively, and S_L and S_T are the longitudinal and shear stresses, respectively.

$$\begin{aligned} F_{mt} &= \left(\frac{\hat{\sigma}_2 + \hat{\sigma}_3}{Y_t}\right)^2 + \frac{\hat{\tau}_{23}^2 - \hat{\sigma}_2\hat{\sigma}_3}{S_T^2} + \frac{\hat{\tau}_{21}^2 + \hat{\tau}_{31}^2}{S_L^2} = 1.0 \qquad if\ \hat{\sigma}_2 + \hat{\sigma}_3 \geq 0 \\ F_{mc} &= \left[\left(\frac{Y_c}{2S_T}\right)^2 - 1\right]\left(\frac{\hat{\sigma}_2 + \hat{\sigma}_3}{Y_c}\right) + \left(\frac{\hat{\sigma}_2 + \hat{\sigma}_3}{2S_T}\right)^2 + \frac{\hat{\tau}_{23}^2 - \hat{\sigma}_2\hat{\sigma}_3}{S_T^2} + \frac{\hat{\tau}_{21}^2 + \hat{\tau}_{31}^2}{S_L^2} = 1.0 \qquad if\ \hat{\sigma}_2 + \hat{\sigma}_3 < 0 \end{aligned} \tag{25}$$

The third mode is the compressive F_{ic} and tensile F_{it} interlaminar failure criterion (26), in which Z_t and Z_c are the out-of-plane damage tensile and compressive thresholds, respectively. This failure criterion is based on the initial work of [Camanho et al. 1999], with the influence of the shear stresses in the interlaminar plane.

$$\begin{aligned} F_{it} &= \left(\frac{\hat{\sigma}_3}{Z_t}\right)^2 + \left(\frac{\tau_{31}}{S_L}\right)^2 + \left(\frac{\tau_{32}}{S_T}\right)^2 = 1.0 \qquad if\ \hat{\sigma}_3 \geq 0 \\ F_{ic} &= \left(\frac{\hat{\sigma}_3}{Z_c}\right)^2 = 1.0 \qquad if\ \hat{\sigma}_3 < 0 \end{aligned} \tag{26}$$

3.1.2 Onset of Damage Initiation

For this work, the same formulation of equivalent strains and stresses applied in previous 2D Hashin damage models are used [Lapczyk et al. 2007]. These are then updated and assembled for the 3D space using the same MLT (Matzenmiller, Lubliner, and Taylor) for 2D formulation [Matzenmiller et al. 1995], with different equivalent stresses and strains for the fibre, matrix, and interlaminar in tensile and compressive damage evolution [Rahimian Koloor et al. 2020].

The equivalent strain is calculated using general equivalent principal virtual work [Lemaitre et al. 2005], written in the form of (27). For the particular cases of the fibre and matrix directions, these equations are rewritten into (28), (29). The chosen stresses and strains used to compute the equivalent ones $(\sigma_{eq}, \varepsilon_{eq})$, are associated with the full effective stresses present in the respective failure criterion. This last statement is the modification of the proposed 3D Hashin damage model [Arruda et al. 2023], that allows for a full 3D damage evolution behaviour.

The onset of damage is associated with the effective stresses $\hat{\sigma}_{ij}^{onset\_of\_damage}$ before damage occurs in either the fibre, matrix or interlaminar direction. Before the onset of damage, the failure criterion is always smaller than 1.0. The procedure to find the parameter β (30), that is used to determinate the initial stress and strain (31), is fully described in [Lapczyk et al. 2007], and is solve separately for each direction and tensile and compressive behaviour (33).

$$\sigma_{eq}\varepsilon_{eq} = \sum \sigma_{ij}\varepsilon_{ij} \quad \text{and} \quad \varepsilon_{eq} = \sqrt{\sum \varepsilon_{ij}^2} \tag{27}$$

$$\begin{cases} \varepsilon_{eq,ft} = \sqrt{\langle \varepsilon_1 \rangle^2 + \gamma_{12}^2 + \gamma_{13}^2} \\ \varepsilon_{eq,fc} = \langle -\varepsilon_1 \rangle \\ \varepsilon_{eq,mt} = \sqrt{\langle \varepsilon_2 \rangle^2 + \langle \varepsilon_3 \rangle^2 + \gamma_{21}^2 + \gamma_{23}^2 + \gamma_{31}^2} \\ \varepsilon_{eq,mc} = \sqrt{\langle -\varepsilon_2 \rangle^2 + \langle -\varepsilon_3 \rangle^2 + \gamma_{21}^2 + \gamma_{23}^2 + \gamma_{31}^2} \\ \varepsilon_{eq,it} = \sqrt{\langle \varepsilon_3 \rangle^2 + \gamma_{31}^2 + \gamma_{32}^2} \\ \varepsilon_{eq,ic} = \langle -\varepsilon_3 \rangle \end{cases} \tag{28}$$

$$\begin{cases} \sigma_{eq,ft} = \dfrac{\langle\sigma_1\rangle\langle\varepsilon_1\rangle + \tau_{12}\gamma_{12} + \tau_{13}\gamma_{13}}{\sqrt{\langle\varepsilon_1\rangle^2 + \gamma_{12}^2 + \gamma_{13}^2}} \\ \sigma_{eq,fc} = \langle-\sigma_1\rangle \\ \sigma_{eq,mt} = \dfrac{\langle\sigma_2\rangle\langle\varepsilon_2\rangle + \langle\sigma_3\rangle\langle\varepsilon_3\rangle + \tau_{21}\gamma_{21} + \tau_{23}\gamma_{23} + \tau_{31}\gamma_{31}}{\sqrt{\langle\varepsilon_2\rangle^2 + \langle\varepsilon_3\rangle^2 + \gamma_{21}^2 + \gamma_{23}^2 + \gamma_{31}^2}} \\ \sigma_{eq,mc} = \dfrac{\langle-\sigma_2\rangle\langle-\varepsilon_2\rangle + \langle-\sigma_3\rangle\langle-\varepsilon_3\rangle + \tau_{21}\gamma_{21} + \tau_{23}\gamma_{23} + \tau_{31}\gamma_{31}}{\sqrt{\langle-\varepsilon_2\rangle^2 + \langle-\varepsilon_3\rangle^2 + \gamma_{21}^2 + \gamma_{23}^2 + \gamma_{31}^2}} \\ \sigma_{eq,it} = \dfrac{\langle\sigma_3\rangle\langle\varepsilon_3\rangle + \tau_{31}\gamma_{31} + \tau_{32}\gamma_{32}}{\sqrt{\langle\varepsilon_3\rangle^2 + \gamma_{31}^2 + \gamma_{32}^2}} \\ \sigma_{eq,ic} = \langle-\sigma_3\rangle \end{cases} \tag{29}$$

$$\hat{\sigma}_{ij} = \beta\hat{\sigma}_{ij}^{onset\_of\_damage} = \beta\hat{\sigma}_{ij}(d_0) \quad \Longrightarrow \quad \hat{\sigma}_{ij}(d_0) \propto \varepsilon_{ij}(d_0) \tag{30}$$

$$\sigma_i(d_0) = C_{d\,ij}\varepsilon_j(d_0) \tag{31}$$

$$\beta = \frac{-b + \sqrt{b^2 - 4ac}}{2a} \tag{32}$$

$$\begin{cases} F_{ft}(\hat{\sigma}_1, \cancel{\hat{\sigma}_2}, \cancel{\hat{\sigma}_3}, \hat{\tau}_{12}, \hat{\tau}_{13}, \cancel{\hat{\tau}_{23}}) = 0 \Rightarrow \beta_{ft} \\ F_{fc}(\hat{\sigma}_1, \cancel{\hat{\sigma}_2}, \cancel{\hat{\sigma}_3}, \cancel{\hat{\tau}_{12}}, \cancel{\hat{\tau}_{13}}, \cancel{\hat{\tau}_{23}}) = 0 \Rightarrow \beta_{fc} \\ F_{mt}(\cancel{\hat{\sigma}_1}, \hat{\sigma}_2, \hat{\sigma}_3, \hat{\tau}_{21}, \hat{\tau}_{31}, \hat{\tau}_{23}) = 0 \Rightarrow \beta_{mt} \\ F_{mc}(\cancel{\hat{\sigma}_1}, \hat{\sigma}_2, \hat{\sigma}_3, \hat{\tau}_{21}, \hat{\tau}_{31}, \hat{\tau}_{23}) = 0 \Rightarrow \beta_{mc} \\ F_{it}(\cancel{\hat{\sigma}_1}, \cancel{\hat{\sigma}_2}, \hat{\sigma}_3, \cancel{\hat{\tau}_{12}}, \hat{\tau}_{31}, \hat{\tau}_{32}) = 0 \Rightarrow \beta_{it} \\ F_{ic}(\cancel{\hat{\sigma}_1}, \cancel{\hat{\sigma}_2}, \hat{\sigma}_3, \cancel{\hat{\tau}_{12}}, \cancel{\hat{\tau}_{13}}, \cancel{\hat{\tau}_{23}}) = 0 \Rightarrow \beta_{it} \end{cases} \tag{33}$$

3.2 3D Tsai-Wu based Damage Model

Previously, in the work of [Arruda et al. 2021], an initial 2D formulation with only plane damage evolution depending on a 2D plane tensor was adopted. This formulation presented some limitations when damage shear evolution happened in both tensile and compressive behaviour for the fibre and matrix failure modes, which led to a different damage shear function. To standardize the Hashin and Tsai-Wu based damage models, this formulation is written in a full 3D strain tensor, therefore maintaining the classical shear damage evolution in orthotropic materials.

3.2.1 Tsai-Wu Failure Criterion

The Tsai-Wu theory is based on a classical stress tensor polynomial failure criterion for the general strength of anisotropic materials, as generically defined by equation (34). In this work, in order to verify the increase of the Tsai-Wu index (34) associated with the increase of strains, the effective stresses $\hat{\sigma}_i$, defined by equation (3), are used.

$$\begin{aligned} F_1\hat{\sigma}_1 + F_2\hat{\sigma}_2 + F_3\hat{\sigma}_3 + 2F_{12}\hat{\sigma}_1\hat{\sigma}_2 + 2F_{13}\hat{\sigma}_1\hat{\sigma}_3 + 2F_{23}\hat{\sigma}_2\hat{\sigma}_3 + F_{11}\hat{\sigma}_1^2 + F_{22}\hat{\sigma}_2^2 + F_{33}\hat{\sigma}_3^2 + F_{66}\hat{\tau}_{12}^2 \\ + F_{55}\hat{\tau}_{13}^2 + F_{44}\hat{\tau}_{23}^2 = TW\left(\hat{\sigma}_i, F_{jk}\right) = 1.0 \end{aligned} \tag{34}$$

$$F_{TW} = TW(\hat{\sigma}_i, F_{jk}) - 1 = 0 \tag{35}$$

In equation (35), the terms F_i and F_{ii}, defined by equations (36) and (37), are second order strength tensors and are related to the one directional engineering strengths, which are easily measured in laboratory. The interaction term F_{ij} is provided by biaxial test conditions, and according to some early theories, these must be selected with caution to obtain accurate values for the strength tensors [Tsai et al. 1971] (39), (40) and (41). These terms must obey the inequality defined in equation (42) to ensure a definition of a closed surface for which it is possible to demonstrate that for isotropic materials, if F_{ij} obeys equation (43), the classical Von-Mises criterion is recovered. The material parameters depend on the stress direction and sign: X_t and Y_t are the tension limit strength of the fibre and matrix, respectively; X_c and Y_c are the compression limit strength of the fibre and matrix, respectively; S_L corresponds to the longitudinal shear resistance; S_T is the transverse shear resistance; and S_I is the interlaminar shear resistance.

$$F_{11} = \frac{1}{X_t X_c} \quad F_{22} = \frac{1}{Y_t Y_c} \quad F_{33} = \frac{1}{Z_t Z_c} \tag{36}$$

$$F_1 = \frac{1}{X_t} - \frac{1}{X_c} \quad F_2 = \frac{1}{Y_t} - \frac{1}{Y_c} \quad F_3 = \frac{1}{Z_t} - \frac{1}{Z_c} \tag{37}$$

$$F_{44} = \frac{1}{S_I^2} \quad F_{55} = \frac{1}{S_T^2} \quad F_{66} = \frac{1}{S_L^2} \tag{38}$$

$$F_{12} = \frac{1}{2B_{t,12}^2}\left(1 - B_{t,12}(F_1 + F_2) - B_{t,12}^2(F_{11} + F_{22})\right) \tag{39}$$

$$F_{13} = \frac{1}{2B_{t,13}^2}\left(1 - B_{t,13}(F_1 + F_3) - B_{t,13}^2(F_{11} + F_{33})\right) \tag{40}$$

$$F_{23} = \frac{1}{2B_{t,23}^2}\left(1 - B_{t,23}(F_2 + F_3) - B_{t,23}^2(F_{22} + F_{33})\right) \tag{41}$$

$$F_{ij}^2 < F_{ii}F_{jj} \tag{42}$$

$$F_{ij} = -\frac{1}{2}\sqrt{F_{ii}F_{jj}} \tag{43}$$

It is known that some composites do not satisfy condition (42), as referred to in the work of [Li et al. 2017], in which it was also mathematically demonstrated that this condition can be relaxed under some circumstances. In any case, for the range of composites used in this work, the term F_{12} still verifies inequality (42). The main difficulty is to obtain the term $B_{t,xy}$, which is the tensile bi-stress strength. This term can be estimated using the several outputs from the World-Wide Failure Exercise [Kaddour et al. 2013], in which it is possible to obtain a lower-bound estimate using the maximum failure envelope, as written in equation (44). In any case, several authors have proven that the exact value of F_{12} is almost irrelevant for normal engineering applications [Tsai 1984; Tsai et al. 1980], as it only tilts the failure ellipse of the Tsai-Wu function.

$$B_{t,12} = \min\left\{\frac{Y_t}{1 - \nu_{21}}; \frac{X_t}{1 - \nu_{12}}\right\} \tag{44}$$

$$B_{t,13} = \min\left\{\frac{Z_t}{1-\nu_{31}}; \frac{X_t}{1-\nu_{13}}\right\} \tag{45}$$

$$B_{t,23} = \min\left\{\frac{Z_t}{1-\nu_{32}}; \frac{Y_t}{1-\nu_{23}}\right\} \tag{46}$$

3.2.2 Onset of Damage Initiation

$$\hat{\sigma}_{ij} = \beta\hat{\sigma}_{ij}^{onset\_of\_damage} = \beta\hat{\sigma}_{ij}(d_0) \quad \Longrightarrow \quad \hat{\sigma}_{ij}(d_0) \propto \varepsilon_{ij}(d_0) \tag{47}$$

$$\sigma_i(d_0) = C_{d_{ij}}\varepsilon_j(d_0) \tag{48}$$

$$\beta^2 \underbrace{(2F_{12}\hat{\sigma}_1\hat{\sigma}_2 + 2F_{13}\hat{\sigma}_1\hat{\sigma}_3 + 2F_{23}\hat{\sigma}_2\hat{\sigma}_3 + F_{11}\hat{\sigma}_1^2 + F_{22}\hat{\sigma}_2^2 + F_{33}\hat{\sigma}_3^2 + F_{66}\hat{\tau}_{12}^2 + F_{55}\hat{\tau}_{13}^2 + F_{44}\hat{\tau}_{23}^2)}_{a} + \beta \underbrace{(F_1\hat{\sigma}_1 + F_2\hat{\sigma}_2 + F_3\hat{\sigma}_3)}_{b} + \underbrace{(-1)}_{c} = 0 \tag{49}$$

$$\beta = \frac{-b + \sqrt{b^2 - 4ac}}{2a} \tag{50}$$

To define the damage evolution constitutive laws, it is necessary to compute the initial equivalent stresses, σ_{eq}^0, and the initial equivalent strains, ε_{eq}^0, defined in section 4.2. It is necessary to solve the Tsai-Wu criterion for the onset of damage initiation as defined by equation (35), which corresponds to the second degree equation (49), with β (50). After this, it is possible to compute the stress and strain fields at the onset of damage, and its equivalent quantities, as defined in equations (47). After calculating the strain field at the onset of damage, it is possible to use the constitutive relation law (38), to compute the given stress field to be used in the equivalent stress (29).

$$\begin{cases} F_{TW}(\langle\hat{\sigma}_1\rangle, \cancel{\hat{\sigma}_2}, \cancel{\hat{\sigma}_3}, \hat{\tau}_{12}, \hat{\tau}_{13}, \cancel{\hat{\tau}_{23}}) = 0 \Rightarrow \beta_{ft} \\ F_{TW}(\langle-\hat{\sigma}_1\rangle, \cancel{\hat{\sigma}_2}, \cancel{\hat{\sigma}_3}, \cancel{\hat{\tau}_{12}}, \cancel{\hat{\tau}_{13}}, \cancel{\hat{\tau}_{23}}) = 0 \Rightarrow \beta_{fc} \\ F_{TW}(\cancel{\hat{\sigma}_1}, \langle\hat{\sigma}_2\rangle, \langle\hat{\sigma}_3\rangle, \hat{\tau}_{12}, \hat{\tau}_{13}, \hat{\tau}_{23}) = 0 \Rightarrow \beta_{mt} \\ F_{TW}(\cancel{\hat{\sigma}_1}, \langle-\hat{\sigma}_2\rangle, \langle-\hat{\sigma}_3\rangle, \hat{\tau}_{12}, \hat{\tau}_{13}, \hat{\tau}_{23}) = 0 \Rightarrow \beta_{mc} \\ F_{TW}(\cancel{\hat{\sigma}_1}, \cancel{\hat{\sigma}_2}, \langle\hat{\sigma}_3\rangle, \cancel{\hat{\tau}_{12}}, \hat{\tau}_{13}, \hat{\tau}_{23}) = 0 \Rightarrow \beta_{it} \\ F_{TW}(\cancel{\hat{\sigma}_1}, \cancel{\hat{\sigma}_2}, \langle-\hat{\sigma}_3\rangle, \cancel{\hat{\tau}_{12}}, \cancel{\hat{\tau}_{13}}, \cancel{\hat{\tau}_{23}}) = 0 \Rightarrow \beta_{it} \end{cases} \tag{51}$$

For each of the principal material directions, fiber, matrix and interlaminar in tension and compression, it is necessary to separately solve the Tsai-Wu damage initiation criterion, as referred to in equations (51). The choice of these stress planes is related to the general assumption that the damage evolution depends mainly on the stresses and strains belonging to the same damage variable plane. This is in accordance to many other orthotropic damage models published earlier [Wang et al. 2017].

3.2.3 State Direction Variable

$$z_{ft} = \frac{\langle\hat{\sigma}_1\rangle}{X_t} + \frac{|\hat{\tau}_{12}|}{S_L} + \frac{|\hat{\tau}_{13}|}{S_T} \qquad z_{fc} = \frac{\langle-\hat{\sigma}_1\rangle}{X_c} \tag{52}$$

$$z_{mt} = \frac{\langle \hat{\sigma}_2 \rangle}{Y_t} + \frac{\langle \hat{\sigma}_3 \rangle}{Z_t} + \frac{|\hat{\tau}_{21}|}{S_L} + \frac{|\hat{\tau}_{31}|}{S_T} + \frac{|\hat{\tau}_{23}|}{S_I} \quad z_{mc} = \frac{\langle -\hat{\sigma}_2 \rangle}{Y_t} + \frac{\langle -\hat{\sigma}_3 \rangle}{Z_t} + \frac{|\hat{\tau}_{21}|}{S_L} + \frac{|\hat{\tau}_{31}|}{S_T} + \frac{|\hat{\tau}_{23}|}{S_I} \tag{53}$$

$$z_{it} = \frac{\langle \hat{\sigma}_3 \rangle}{Z_t} + \frac{|\hat{\tau}_{13}|}{S_T} + \frac{|\hat{\tau}_{32}|}{S_I} \quad z_{mc} = \frac{\langle -\hat{\sigma}_3 \rangle}{Z_t} \tag{54}$$

The state direction variable z is defined for the fibre, matrix, and interlaminar tension and compression behaviour by equations (52), (53), and (54) respectively. This state direction variable is necessary in order to guarantee that when the Tsai-Wu criterion is reached, only some damage modes are activated at the same time. This state variable also guarantees that in the presence of an uniaxial stress state, only one damage mode is activated, preserving the thermodynamics of the problem, something other damage models are not able to simulate. The effective stresses are used in order to guarantee that the state variable always increases. As mentioned, equivalent strains were not chosen in order to prevent multi damage modes in uniaxial stress.

$$d^z_{fmi,tc} = z_{fmi,tc} d_{fmi,tc} \tag{55}$$

$$0 \leq z_{fmi,tc} \leq 1 \quad \delta z_{fmi,tc} \geq 0 \quad \delta d^z_{fmi,tc}\left(z_{fmi,tc} > 0\right) \geq 0 \tag{56}$$

The damage variable computed using equation (55) is then corrected using equation (56), where the state direction variable is used in order to prevent the damage growth on a certain plane axis where the stress is not that prevalent. In any case, in the presence of biaxial stress states, the damage variables evolve just like in other damage models. In order to promote the thermodynamic admissibility of the damage model, the state variable must verify the conditions (20), that are now rewritten in equation (56) for the fibre, matrix, and interlaminar tension and compression behaviours.

3.3 Damage Evolution

To alleviate mesh dependency that may occur with material softening, a characteristic length L_c is introduced into the formulation so that the constitutive law is expressed as a stress-equivalent displacement relation [Lopes et al. 2020]. In this work, it is considered that the characteristic length is computed as the square root of the numerically computed surface area. The equivalent displacement definitions (57) are the same as the ones initially found in the work of [Bazant et al. 1983], which do not depend on the crack direction. This last statement is even more important in orthotropic damage models since the damage evolution will always depend on either the fibre or matrix behaviour. It has been demonstrated in several works , if the mesh is not regular and the stress field distribution is non-uniform, some element dependency/sensitivity is predictable as a consequence of FEM with softening [Lopes et al. 2020; Oliver 1989].

The “evolution law” is then rewritten and takes the final form represented in Figure 1, in which the area $\widehat{\mathrm{ABC}} \Rightarrow \left(\varepsilon_{eq}(d=0)\right)$ under the curve corresponds to the fracture energy G_f. At the moment, new experimental methodologies exist to calculate fracture energy [Forero et al. 2021], but for orthotropic materials, the classical Compact Tension test is still suggested.

The initial values σ^0_{eq} and δ^0_{eq} are calculated at the onset of damage by analytically solving equations (33), and (51), in which the methodology is fully described in [Lapczyk et al. 2007]. In order to obey the Kuhn-Tucker equations, after the beginning of each incremental process, the “evolution law” is updated to curve $\widehat{\mathrm{ADC}} \Rightarrow \left(\varepsilon_{eq}(d)\right)$.

Pre-Print of Mechanics of Advanced Materials and Structures 2023
https://doi.org/10.1080/15376494.2023.2277849

After the damage initiation criterion, beyond point B, it is demonstrated in [Matzenmiller et al. 1995], that for a linear softening evolution, the damage variables are calculated according to equation (58), depending on the fibre or matrix and on tension or compression.

$$\delta_{ij}^{eq} = L_c \varepsilon_{ij}^{eq} \quad and \quad \delta_{eq}^{u} = 2G_f/\sigma_{eq} \tag{57}$$

$$d = \frac{\delta_{eq}^{u}\left(\delta_{eq} - \delta_{eq}^{0}\right)}{\delta_{eq}\left(\delta_{eq}^{u} - \delta_{eq}^{0}\right)} \quad if \quad \delta_{eq}^{0} \le \delta_{eq} \le \delta_{eq}^{u} \tag{58}$$

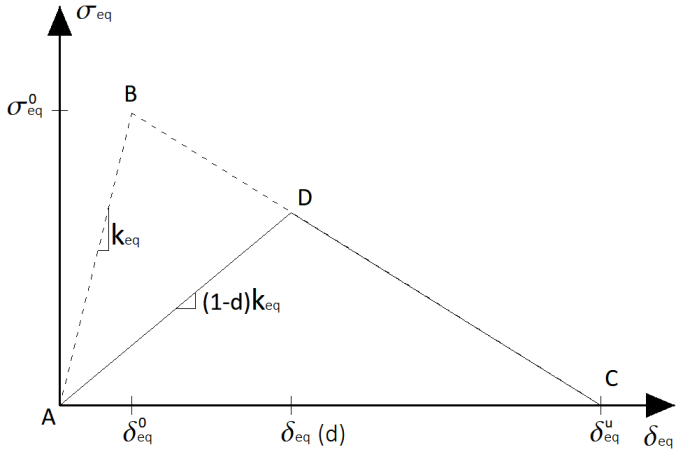

Figure 1 – Constitutive relation for the equivalent stress and equivalent displacement.

In this work, it is also adopted the possibility of using equivalent stresses with residual stress is also adopted, which is important mainly when compression is high and very present in the structural response. Also, to promote some numerical stability, is recommended to use a tensile residual stress that may vary from 1% to 10% of its initial peak value. The adopted residual equivalent stress formulation in Figure 2 is adopted (59) and a new damage function is assembled during the residual equivalent stress segment after point D (60).

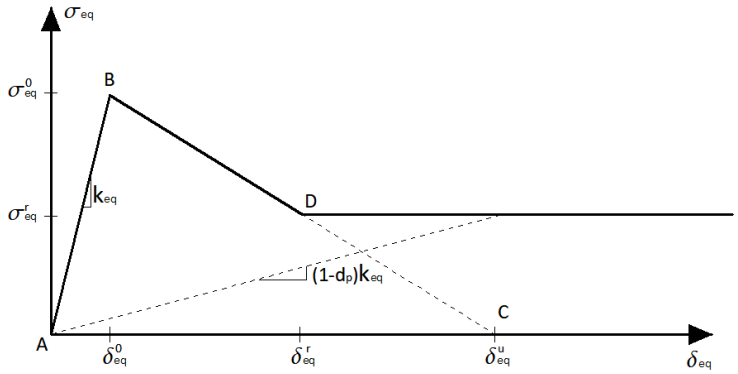

Figure 2 – Constitutive relation with residual stress for the equivalent stress and equivalent displacement.

$$\begin{cases} \sigma_{eq}^{r} = (1-d_D)k_{eq}\delta_{eq}^{D} = (1-d_D)\dfrac{\delta_{eq}^{D}}{\delta_{eq}^{0}}\sigma_{eq}^{0} = \%\sigma_{eq}^{0} \\ (1-d_D) = \dfrac{\delta_{eq}^{0}\left(\delta_{eq}^{u}-\delta_{eq}^{D}\right)}{\delta_{eq}^{D}\left(\delta_{eq}^{u}-\delta_{eq}^{0}\right)} \end{cases} \Rightarrow \delta_{eq}^{D} = \delta_{eq}^{u} - \%\left(\delta_{eq}^{u}-\delta_{eq}^{0}\right) \tag{59}$$

$$\begin{aligned} &\sigma_{eq} = (1-d_r)k_{eq}\delta_{eq} = \sigma_{eq}^{r} = \%\sigma_{eq}^{0} \\ &\Leftrightarrow (1-d_r)\frac{\sigma_{eq}^{0}}{\delta_{eq}^{0}}\delta_{eq} = \%\sigma_{eq}^{0} \\ &\Leftrightarrow d_r = 1 - \%\frac{\delta_{eq}^{0}}{\delta_{eq}} \end{aligned} \tag{60}$$

4 Convergence Procedures

4.1 Viscous Regularization

When using only the energy regularization described in the previous section, some issues are still left that may cause: (i) loss of positive definiteness of the tangent stiffness; (ii) some localization of damage; and (iii) some numerical convergence difficulties. To overcome these problems, an efficient and simple procedure is to implement viscous regularization.

When the tangent stiffness tensor is not positive definite, damage localizes in a narrow band, and the numerical solution depends upon the numerical discretization, in which decreasing the element size in the localized zone decreases the computed energy dissipated [Srinivasa et al. 2022]. Therefore, the structural response is not objective because it does not converge to a unique solution with mesh refinement. Also when the tangent stiffness is not positive definite, standard Newton-Rapshon techniques present convergence difficulties [Borst et al. 2012], no quadratic convergence is guaranteed.

As referred to above, it is possible to overcome some of these convergence difficulties by using the viscous regularization scheme. This numerical algorithm is based on an artificial Duvaut-Lions viscosity model [Duvaut et al. 1972], and more details on the theoretical background of this method can be found in the work of [Geers et al. 1994]. This algorithm causes the tangent stiffness matrix of the softening material to be positive definite for sufficiently small time increments, improving the convergence. In the limit the secant matrix is fully recovered. In this regularization scheme, a viscous damage variable is defined by the evolution equation (61).

$$\delta d_v = \frac{1}{\eta}(d - d_v) \times \delta_t \tag{61}$$

Where d is the damage variable obtained as described previously, d_v is the regularized viscous damage variable, and η is the viscosity stabilization factor. The damage response of the viscous material is given as (62), and the non-damage response is given as (63).

$$\{\sigma_v\} = [C_d^v]\{\varepsilon\} \tag{62}$$

$$\{\sigma\} = [C_d]\{\varepsilon\} \tag{63}$$

The damaged elastic matrix, C_d^v, is computed using the viscous values of damage variables for each failure mode. Using viscous regularization with a small value for the viscosity parameter (small compared to the characteristic time increment) usually helps improving the rate of convergence of the model in the softening regime without compromising the quality of the numerical solution. The basic idea is that the solution of the viscous system relaxes to that of the inviscid case as $\eta \to 0$, where t represents time. A numerical algorithm needs to be implemented for the time integration of the internal variables. Using a backward-Euler scheme [Dunne et al. 2005], the internal variables can be updated, resulting in the viscous damage variable (64), by combining it with the previous expression (61).

$$d_v^{t+\Delta t} = d_v^t + \Delta d_v^t \Longrightarrow d_v^{t+\Delta t} = d_v^t + \frac{1}{\eta}(d^{t+\Delta t} - d_v^{t+\Delta t}) \times \Delta_t \tag{64}$$

It is now possible to compute the viscous damage using the information from the previous viscous damage and the current non-viscous damage (65), retaining the implicit time integration.

$$d_v^{t+\Delta t} = \frac{\eta}{\eta + \Delta \mathrm{t}} d_v^t + \frac{\Delta \mathrm{t}}{\eta + \Delta \mathrm{t}} d^{t+\Delta t} \tag{65}$$

It is important to guarantee that the level of viscosity is not too high, this is performed indirectly by comparing the level of elastic damaged energy (66), and the viscous energy dissipation (67), in which the first must always override the second. If the time step Δt is very small, it is possible that the first term of the sum in (67) overrides the second, providing an increase of viscous energy dissipation that may compromise the accuracy of the numerical results.

$$E_d^{t+\Delta t} = E_d^t + \frac{1}{2}\left[\sum_{i=1}^{n} \left(\sigma_{v,i}^{t+\Delta t} + \sigma_{v,i}^t\right) \Delta\varepsilon_i\right] \tag{66}$$

$$E_v^{t+\Delta t} = E_v^t + \frac{1}{2}\left[\sum_{i=1}^{n} \left(\sigma_{v,i}^{t+\Delta t} + \sigma_{v,i}^t - \sigma_i^{t+\Delta t} - \sigma_i^t\right) \Delta\varepsilon_i\right] \tag{67}$$

4.2 Predictor-Corrector Implicit to Explicit

Some authors have user UMAT user-subroutines in ABAQUS without resourcing to a fully Jacobi stiffness matrix (vtangent matrix), using only a secant matrix for the ABAQUS predictor-corrector with viscous regularization.

As referred to before, viscous regularization has only been demonstrated to be a fully implicit method when a tangent matrix is used for the predictor-corrector [Chaboche et al. 2001; Geers et al. 1994]. The use of secant matrix with viscous regularization lacks the theoretical background to prove its implicit convergence. It can be seen in expression (65), that if the time step is larger than the viscosity parameter $\Delta t \gg \eta$, then the level of regularization is low enough, and the implicit standard convergence can be admitted since the viscous damage is always related to the current time step as the non-viscous damage. However, if the time step is lower than the viscosity parameter $\Delta t \ll \eta$ then the viscous damage will always be related to the previous time step, therefore promoting and explicit time step integration.

This last case can cause some conflicts since the strain increment follows a full implicit integration scheme (68). These inconsistencies happen when damage follows an explicit time step update $d_v^{t+\Delta t} \simeq d_v^t$, and the strain increment follows a full implicit integration scheme. This can cause some convergence problems, especially if the time step is very small $\Delta t \ll \eta$. Also, when the time step is very small since the

Pre-Print of Mechanics of Advanced Materials and Structures 2023
https://doi.org/10.1080/15376494.2023.2277849

viscous damage solution overrides the non viscous damage solution, the viscous damage energy tends to grow (67), indirectly providing extra energy which is not real.

$$\varepsilon_{t+\Delta t} = \varepsilon_t + \Delta\varepsilon_{t+\Delta t} \tag{68}$$

To solve this problem, a new implicit to explicit algorithm is proposed, in which the fundamental basis guarantees that when the time step is large, the damage evolution follows an implicit time step integration, but when the time step is smaller than the viscosity parameter, then the damage evolution switches to an explicit time step integration. This is an optimization of the predictor-corrector of ABAQUS, that states when the time step is large enough a full implicit formulation is used, but when the predictor-corrector algorithm of ABAQUS presents complications in converging, reducing the time step, then an explicit formulation is used to supress the converging difficulty. The basis of this formulation is using the increment correction parameter ϖ linked to the portion of the non-viscous damage variable $d^{t+\Delta t}$ in expression (69).

$$\varepsilon_{t+\Delta t} = \varepsilon_t + \varpi \times \Delta\varepsilon_{t+\Delta t} \tag{69}$$

In which:

$$\varpi = \frac{\Delta t}{\Delta t + \eta} \tag{70}$$

It is important to point out that when $\varpi = 1.0$ the material stiffness and stress update during the time integration in the UMAT follows a full implicit formulation, on the contrary, when $\varpi = 0.0$ it follows a full explicit time integration for the material stiffness and stress update.
Using this algorithm, it is guaranteed that when performing the viscous regularization, if the predictor-corrector uses large time steps, both the viscous and non-viscous solution portions of the expression (65) will contribute to the implicit time step integration. But, when the time step is small enough, then the increment correction parameter tends to be small, close to an explicit integration, and the influence of the non-viscous solution overrides the viscous solution, therefore using only the previous damage variable. This way, there is no mixed implicit time step integration with previous step damage variables, as suggested before, that may compromise the convergence and accuracy of the numerical solution.

To better understand the variation of ϖ with Δt for a fixed $\eta = 10^{-5}$, it is depicted in Figure 3 a) a graph, in which it is possible to see that even for small times steps from $\Delta t = 10^{-3}$ to $\Delta t = 10^{-5}$, the value of $\varpi > 50\%$, therefore guaranteeing some influence of the $\Delta\varepsilon_{t+\Delta t}$ in the final strain increment $\varepsilon_{t+\Delta t}$. This does not assurances a full implicit behaviour, but is close to it. As depicted in Figure 3 b) using logarithmic scale only when the $\Delta t < 10^{-6}$ the value of $\varpi < 10\%$, being near an explicit form, but still with some influence of $\Delta\varepsilon_{t+\Delta t}$ in the final strain increment $\varepsilon_{t+\Delta t}$.

In conclusion, the algorithm tends to be more implicit when $\Delta t > \eta$, and on the other hand more explicit when $\Delta t < \eta$. In any case, this last situation is not problematic since for very small time steps $\Delta t \ll 10^{-6}$, an explicit solution may still provide good and accurate numerical results. It is important to state that this algorithm admits that the damage variable from the current time step $d^{t+\Delta t}$ is always saved for the next time step, otherwise, viscous damage would never be updated, during the incremental processes.

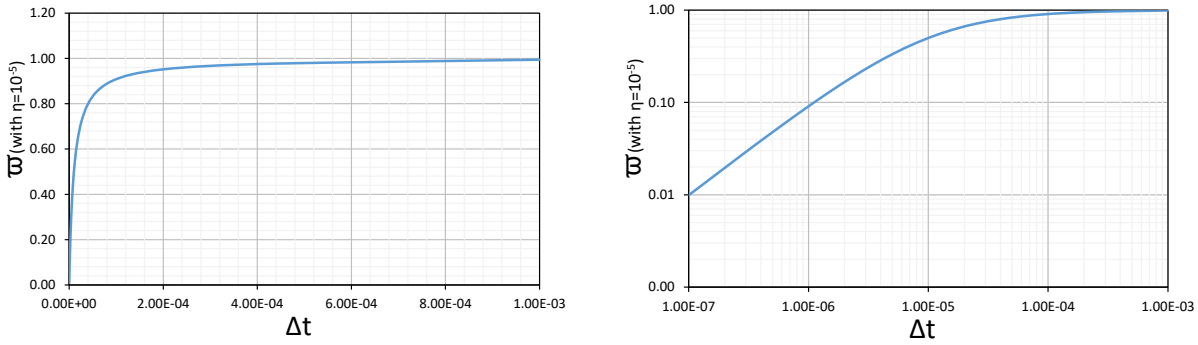

a) Normal Scale b) Logarithmic Scale

Figure 3 – Variation of the correction parameter with the time step increment. (a) normal scale; (b) logarithmic scale.

It is important to point out that expression (69) is only used to update the damage variables, however, for the stress update, expression (68) is always used, even for explicit integration if not, the internal forces wouldn't be in equilibrium.

5 Numerical Tests

In this section, the results from the experimental campaign of [Martins et al. 2021] and [Almeida-Fernandes et al. 2020b] with GFRP specimens and connections are tested and compared with the proposed damage models. These experimental results are fundamental to validate numerical models since they tested most of the material properties, including fracture energy, which is fundamental for correctly numerically simulate the post peak behaviour of materials with softening. Most of these experimental campaigns have also been verified with previous numerical tests in the works of [Almeida-Fernandes et al. 2020a; Arruda et al. 2021].

For numerical tests, it was admitted a total time analysis of 1.0 seconds, due to the non-linear analysis being static, and all time step increments should have a minimum of 0.001 seconds, which is 100 times bigger than the adopted viscosity parameter $\eta = 10^{-5}$.

5.1 Compact Tension Test

The compact tension test is a traditional test to estimate fracture energy, usually in isotropic metals [Chell et al. 1976], and has recently extended to also estimate fracture energy in orthotropic GFRP specimens [Almeida-Fernandes et al. 2020b]. A full description of the experimental campaign for the tensile compact test can be found at [Almeida-Fernandes et al. 2020b], including the description of the imposed displacement in the test setup.

The specimen geometry, test setup, and supporting conditions are all depicted in Figure 4. For the adopted mesh, to reduce the computational cost, the zone outside the notch was modelled with linear orthotropic GFRP behaviour that already existed in the ABAQUS material library. The extra part of the notch was simulated with the proposed UMAT, in which the fracture will occur. These two used different meshes since the zone of the notch needs extra refinement, and later they were connected using tie constrains. The circular supports were modelled with linear isotropic steel also presented in the ABAQUS material library ($E_S = 195GPa, \nu = 0.3$). The contact between the supports and the GFRP specimen was simulated with hard a contact formulation and a friction coefficient of 0.2.

To reduce even further the computational cost, only half of the thickness was simulated, therefore, transversal symmetry conditions were implemented. Figure 5. When the mesh was generated, it was imposed geometries near cubes for all solid finite elements, and several meshes were tested to prevent any mesh dependency.

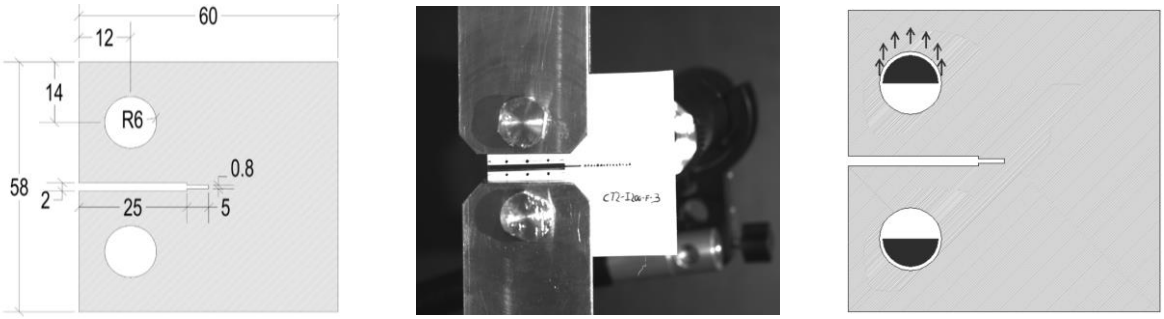

a) Geometry [mm] b) Experimental Layout c) Laboratory Conditions

Figure 4 – Geometry and test setup for the classical compact tension test (CT) [Almeida-Fernandes et al. 2020b].

A 3D non-linear analysis was performed using the ABAQUS standard with C3D8 solid finite elements using full integration and hourglass control. It was observed during the previous experimental campaign that the structural response produced softening, therefore, displacement control was used during the applied vertical load. All the material properties of the GFRP are in Table 1 and

Table 2, and these were obtained in the experimental campaign of [Almeida-Fernandes et al. 2020b]. For the interlaminar material properties, they were admitted to be the same as the matrix properties, due to some isotropic behaviour in the transverse direction.

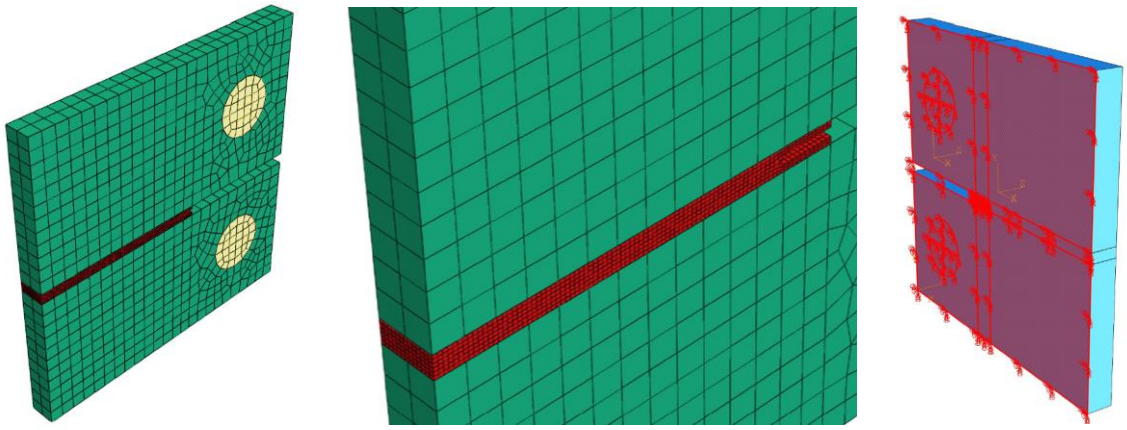

a) b) c)

Figure 5 – Adopted 3D mesh and symmetry conditions for the CT test.

Table 1 – Materials Properties for the pultruded GFRP material used in the CT tests.

$E_1[MPa]$	$E_2[MPa]$	$E_3[MPa]$	$G_{12}[MPa]$	$G_{13}[MPa]$	$G_{23}[MPa]$
29600	11900	11900	2900	3000	3000
$\nu_{12}[-]$	$\nu_{13}[-]$	$\nu_{23}[-]$	$X_t[MPa]$	$X_c[MPa]$	$Y_t[MPa]$
0.27	0.27	0.30	323	426	71
$Y_c[MPa]$	$Z_t[MPa]$	$Z_c[MPa]$	$S_L[MPa]$	$S_T[MPa]$	$S_l[MPa]$
121	71	121	64	67	67

Table 2 – Fracture energy for the pultruded GFRP material used in the CT tests.

$G_{ft}[MPa.mm]$	$G_{fc}[MPa.mm]$	$G_{mt}[MPa.mm]$	$G_{mc}[MPa.mm]$	$G_{it}[MPa.mm]$	$G_{ic}[MPa.mm]$
100	100	20	20	20	20

These tests used the ITE algorithm, with the correction parameter of expression (70). It is important to point out that the UMAT was used for the GFRP, with ABAQUS standard, so the governing system was solved using implicit predictor-correct algorithm for the three tests.

By observing Figure 6, it is important to realize that all tests provided the same structural response, even during the softening branch. The stiffness is the same in all three tests, but the maximum force is a slightly higher in the 2nd test with Tsai-Wu as expected, and reported in [Arruda et al. 2021]. All numerical models present the maximum vertical force, which in some cases is higher than the experimental campaign, but this was also observed by other authors [Xiong et al. 2022]. It is also depicted in Figure 6, the numerical response of a finite element model using a 2D Hashin formulation accessible in the ABAQUS material library by [Almeida-Fernandes et al. 2020b]. For this particular case, this numerical model, shows results similar to the Tsai-Wu 3D formulation, in terms of maximum vertical force.

Also in Figure 7, the matrix damage and vertical stress distribution for a given vertical strain are displayed. For the matrix damage evolution, both tests present the same evolution with the vertical strain, but for the vertical stress evolution during the peak, there is a clear difference between the Hashin and Tsai-Wu damage models. In any case, the value of the maximum vertical stress of the Tsai-Wu damage model is near the pure vertical stress value. But, for the evolution of the vertical stress and vertical strain after the peak, there is almost no visible difference between damage models, concluding that the Tsai-Wu formulation promotes similar accuracy when compared with the Hashin formulation. It is also presented in Figure 8 and Figure 9 the final matrix damage field distribution for the two numerical tests, in which the differences are indeed quite small for both tensile and compressive behaviour.

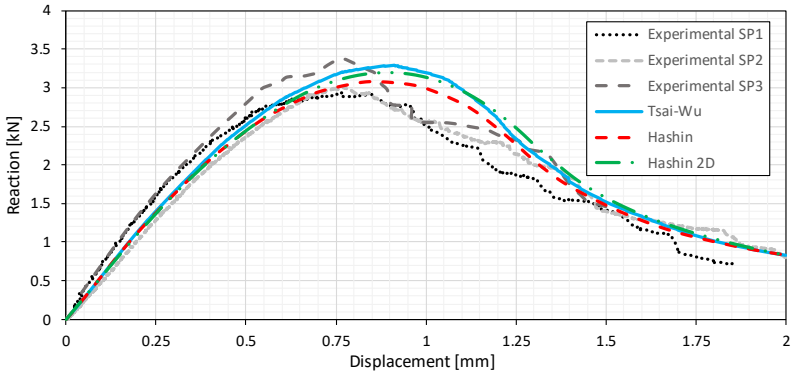

Figure 6 – Vertical force vs displacement, in the load supports for the CT test.

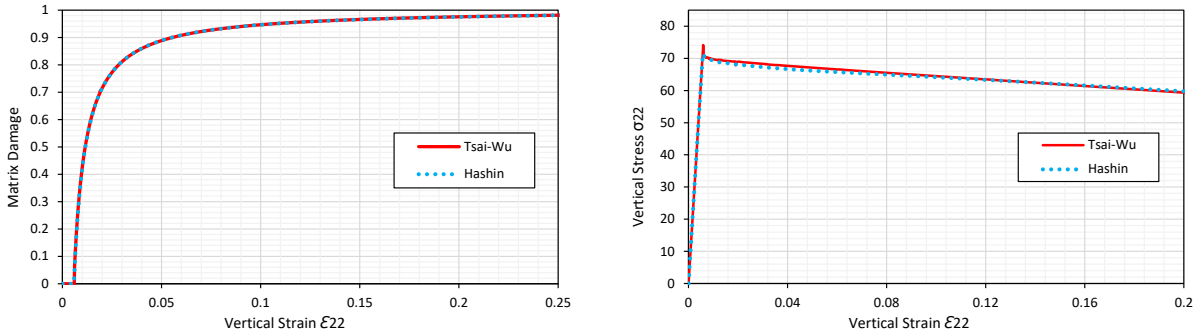

a) b)

Figure 7 – a) damage vs vertical strain, b) vertical stress vs vertical strain, for the CT test.

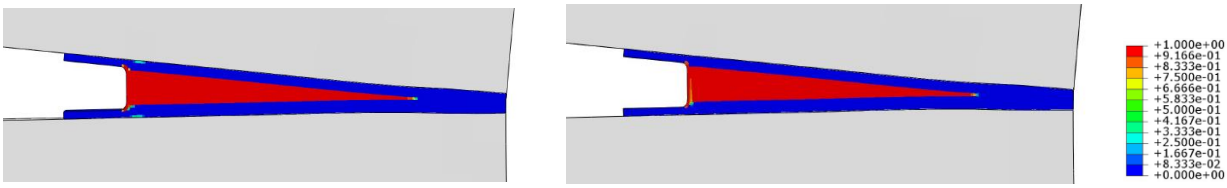

a) b)

Figure 8 – Final tensile matrix damage field distribution for a) Hashin and b) Tsai-Wu based damage formulation.

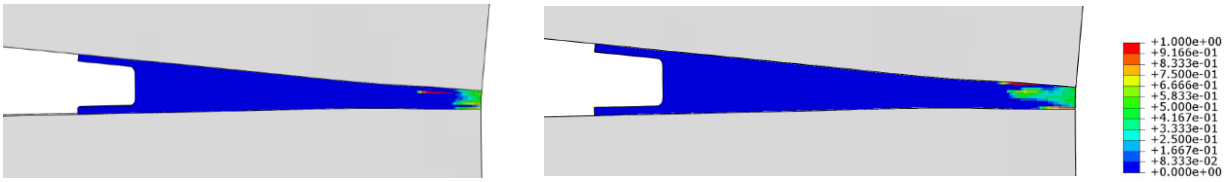

a) b)

Figure 9 – Final compressive matrix damage field distribution for a) Hashin and b) Tsai-Wu based damage formulation.

5.2 Double Lap Test

The double lap test is a standard experiment used to assess the bolt connection between structural elements. The full details of the experimental campaign and test setup are fully described in the work of [Martins et al. 2021], in which it is possible to see the applied load using imposed displacements. Some of the material properties adopted for the numerical test are in Table 3, and these were obtained in the previous referenced work, others were previously estimated by other authors. For the fracture energy, due to some variability in the results, it was used with the same values of the previous numerical tests in Table 2.

For this numerical test, the bolt edge distance (cover) of 15mm and 70mm were simulated, since these clearly show a difference between a shear-out and bearing collapse, respectively (Figure 10). A 3D non-linear analysis was performed with ABAQUS standard using C3D8R solid finite elements with reduce integration and hourglass control. The time step restrictions are the same as in the previous numerical models.

For the GFRP plate, in order to reduce the computational cost, part of the plate near the opening was modelled with the UMAT, but for the other part, an elastic orthotropic material from the ABAQUS library was used. For the steel bolt, an isotropic elastoplastic material from ABAQUS library was used ($E_s = 195GPa, \nu = 0.3, f_y = 300MPa, f_u = 691MPa$). Again, to reduce the computational cost, only ¼ of the structure was simulated, which means ½ of the GFRP plate and one steel plate (Figure 11), in which the imposed vertical displacement is inserted in the bottom of the steel plate.

To correctly simulate the bearing, the residual compressive stress after the maximum peak must also be simulated. The adopted value is 80%, which is the relation between the bearing resistance calculated with [CNR-DT-205/2007 2008], and the compressive resistance provided by [Martins et al. 2021]. Also, to improve convergence, a tensile residual stress of 10% was adopted. A sensitivity test showed that a residual tensile stress below 15% had no influence on the maximum numerical resistance or its softening branch.

Pre-Print of Mechanics of Advanced Materials and Structures 2023
https://doi.org/10.1080/15376494.2023.2277849

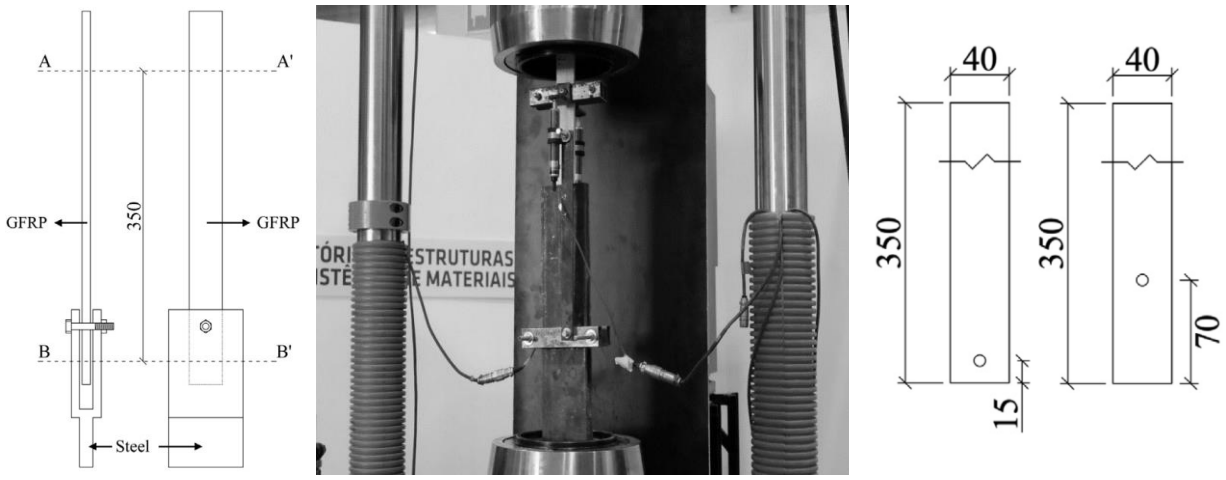

Figure 10 – Test setup for the loading conditions and impose displacement for the double lap test, and used bolt edge distance (cover) for the circular opening [Martins et al. 2021].

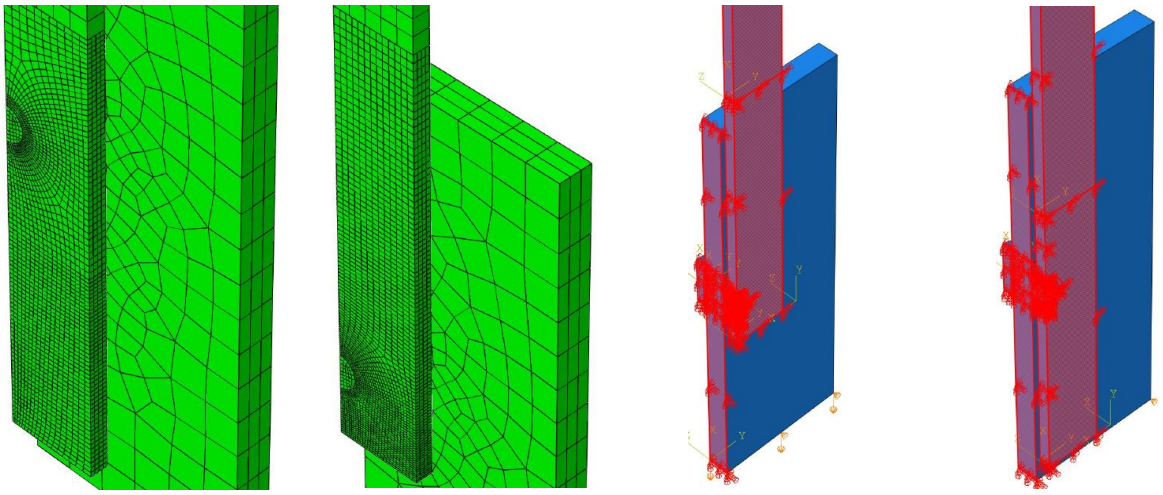

a) b) c) d)

Figure 11 – Adopted 3D mesh and symmetry conditions for the double lap test.

Table 3 – Materials Properties for the pultruded GFRP material used in the double lap tests.

$E_1[MPa]$	$E_2[MPa]$	$E_3[MPa]$	$G_{12}[MPa]$	$G_{13}[MPa]$	$G_{23}[MPa]$
21300	2900	2900	3000	2500	2500
$\nu_{12}[-]$	$\nu_{13}[-]$	$\nu_{23}[-]$	$X_t[MPa]$	$X_c[MPa]$	$Y_t[MPa]$
0.28	0.28	0.30	334.0	316.0	29.0
$Y_c[MPa]$	$Z_t[MPa]$	$Z_c[MPa]$	$S_L[MPa]$	$S_T[MPa]$	$S_l[MPa]$
51.9	29.0	51.9	52.4	33.8	33.8

The structural response of the numerical models and its comparison with the experimental campaign are exhibited in Figure 12 for both 15mm and 70mm covers, for both the Hashin and Tsai-Wu damage models. The vertical force was measured on the steel plate, and the vertical displacement is the relative movement between the steel plate and the GFRP plate. As expected due to the extra flexibility of the experimental test setup, the numerical model is stiffer than the experimental one, this is a common problem when comparing numerical vs experimental structural responses [Martinavičius et al. 2020]. The magnitude of the stiffness in the numerical model was dependent on the adopted final geometry and support conditions, therefore due to its unknown variability, it is not expected to reach the same value as

the one obtained in the experimental campaign. For the 15mm cover, there is a clear overestimation of the maximum reaction for both the Hashin and Tsai-Wu models, which is associated to the tensile matrix resistance and longitudinal 1-2 shear resistance being overestimated. This is expected for the Tsai-Wu failure surface, that may present higher maximum shear resistance, in the presence of a compression stress. Also, the adopted value of the fracture energy was estimated and not measured in an experimental campaign. But, for the 70mm cover, the maximum reaction is nearer the average experimental one since the bearing is the collapse mode, and this is associated with the compressive resistance, which was not estimated.

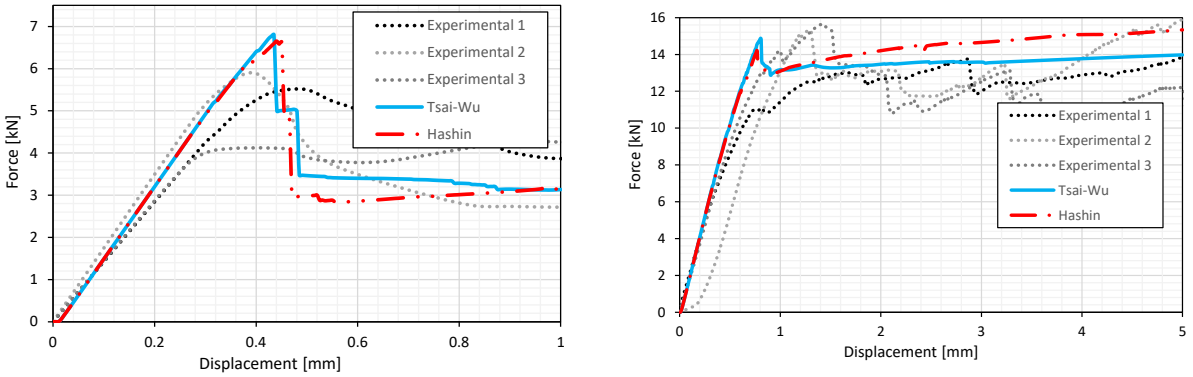

Figure 12 – Final matrix damage field distribution for a) implicit, b) explicit and c) ITE for the double lap test.

It is portrayed in Figure 13, the final shear damage 1-2 field for both numerical models, in which for the 15mm cover it is clearly a full shear-out collapse, but for the 70mm cover there is a bearing collapse followed by a partial shear-out mode that does not finalize Figure 14. This is according to what was observed in the experimental campaign until a relative displacement of 5mm.

Also, only for the 70mm cover can be seen in Figure 14, some difference in the final shear damage field distribution for the Hashin and Tsai-Wu damage models. This is expected since the damage models present different tensile, compressive and shear damage formulation.

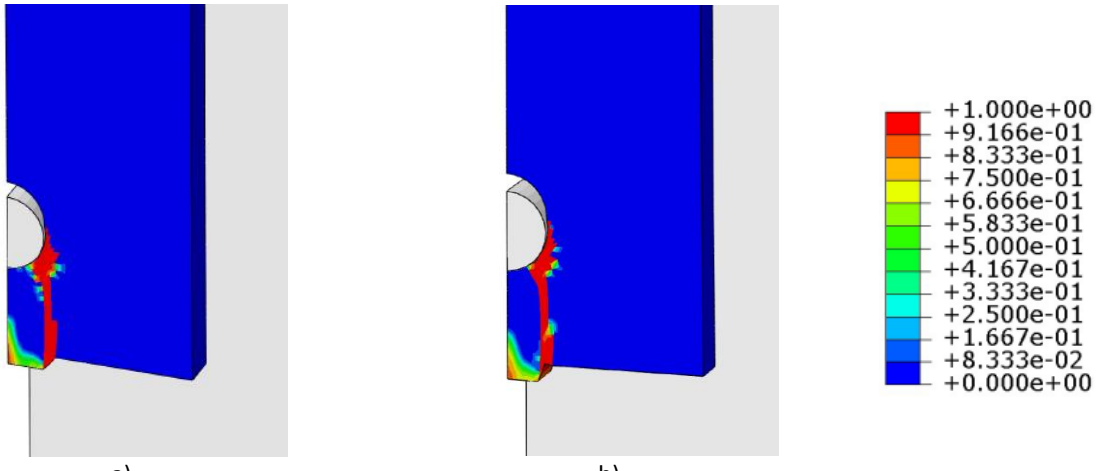

Figure 13 – Final shear damage distribution for 15mm of cover for a) Hashin and b) Tsai-Wu based damage formulation.

Pre-Print of Mechanics of Advanced Materials and Structures 2023
https://doi.org/10.1080/15376494.2023.2277849

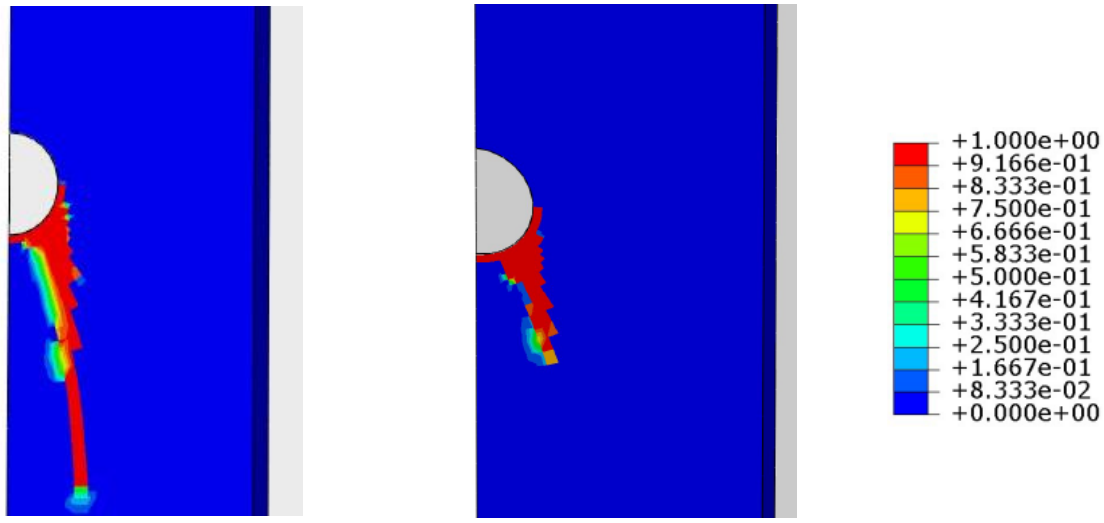

a) b)

Figure 14 – Final shear damage distribution for 70mm of cover for a) Hashin and b) Tsai-Wu based damage formulation.

In Figure 15 a) it is presented the average shear stress and shear damage evolution in the Gauss point nearest the circular opening perimeter at 30° to 45° of the symmetry axis in the GFRP plate, in which the results are presented for both 15mm and 70mm covers. These results are important since they demonstrate that the adoption of a higher residual compressive stress has almost no influence on the residual shear stress. It is possible to observe that the residual shear stress is not near to 20% of the maximum peak. It is mainly associated with the level of cover, which indirectly influences the maximum force in the connection. This is also the case for the shear damage evolution displayed in Figure 15 b).

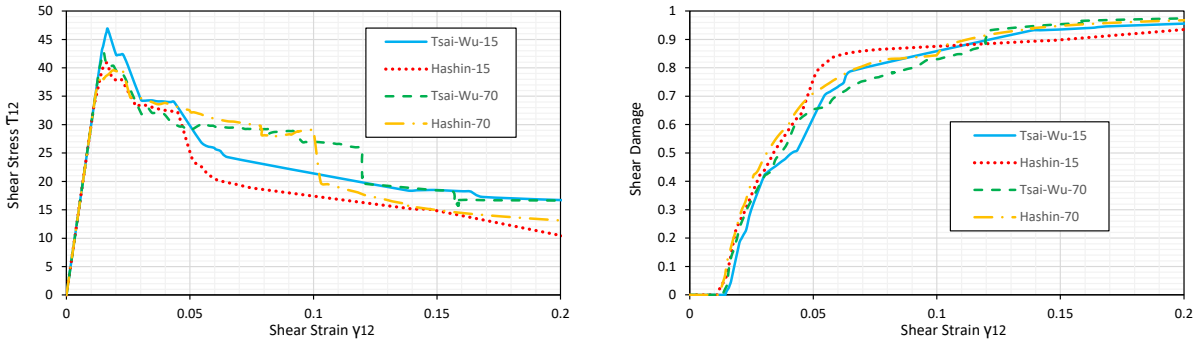

a) b)

Figure 15 – a) average shear stress 12 vs shear distortion 12 and b) average shear damage 12 vs shear distortion 12 in the Gauss point nearest the circular opening perimeter at 30° and 45° of the symmetry axis.

Finally, to better understand that the proposed ITE algorithm does not overestimate the viscous energy and consequently the viscous damage, it is exhibited in Figure 16 the elastic damaged energy (ESE) and the viscous dissipation energy (VSE), for the 15mm cover. As expected, there is a big reduction of force after 0.4s for Hashin Figure 12, and as expected in this case, both the value of ESE and VSE increase, but after a given time step, VSE stabilizes and ESE increases, demonstrating that the VSE is not dominating

the structural response. For the Tsai-Wu damage model, this does not happen, may be due to the force reduction not being instantaneous, which is contrary to what happens in the Hashin damage model.

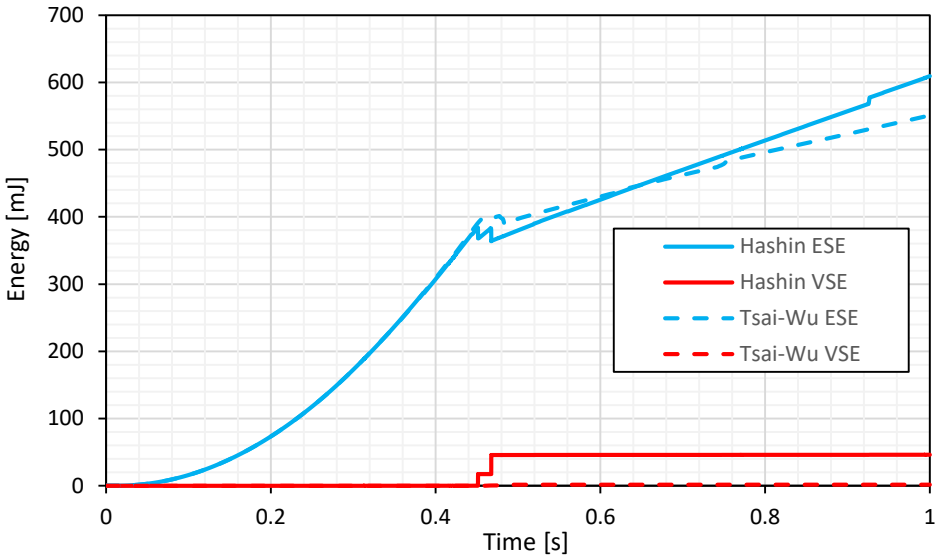

Figure 16 – Total elastic and viscous damage energy for 15mm cover, with both Hashin and Tsai-Wu based damage formulation.

6 Conclusions

The main focus of this study is presenting a new 3D Tsai-Wu based damage model with residual stresses using an implicit to explicit material time integration algorithm to be used in this and future damage models. The study compared this new damage model with a modified Hashin 3D based damage formulation already tested and validated in previous studies. This study was applied and compared with experimental data from already published experimental campaigns with specimens made of GFRP composites.

1) The damage model was able to correctly estimate the structural response of CT, which is useful to correctly simulate the post peak response in materials exhibiting softening behaviour.
2) With the possibility of using residual stress in the orthotropic Tsai-Wu based damage model, it was conceivable to correctly simulate the bearing collapse in GFRP connections.
3) The structural response and final damage distribution were similar in both Hashin and Tsai-Wu based damage formulation, in which the last one provided upper bond results.
4) The Tsai-Wu base damage model provided a more robust iterative model during the convergence process, but with a smaller impact on the final structural response.

6.1 Further Developments

Due to the stress in 3D space with only one single failure criterion for the proposed Tsai-Wu base damage model, the implementation of Mode II shear crack evolution may be easy to implement. For this reason, future numerical implementations will study the possibility of exploring the post-peak shear strain, allowing a shear damage evolution that is not dependent on the fibre, matrix, or interlaminar damage evolution.

6.2 Data Availability

All data and UMAT files will be publicly displayed and ready to be downloaded by the scientific community on GitHub. at *github.com/marioruiarruda/*.

6.3 Acknowledgements

This work was partly supported by Fundação para a Ciência e Tecnologia (FCT) under the Transitional Standard—DL57/2016/N3/UI/CERIS/CT/165/2018.

References

[ABAQUS 2018] ABAQUS.(2018) "*Abaqus Unified FEA-3DEXPERIENCE R2018*". Systèmes, D. Rhode Island, 3DS-SIMULIA.http://www.3ds.com.

[Almeida-Fernandes et al. 2020a] Almeida-Fernandes, L., Silvestre, N., Correia, J. R. and Arruda, M.(2020a) "*Compressive transverse fracture behaviour of pultruded GFRP materials: Experimental study and numerical calibration*." Composite Structures 247: 112453 DOI: https://doi.org/10.1016/j.compstruct.2020.112453.

[Almeida-Fernandes et al. 2020b] Almeida-Fernandes, L., Silvestre, N., Correia, J. R. and Arruda, M. R. T.(2020b) "*Fracture toughness-based models for damage simulation of pultruded GFRP materials*." Composites Part B: Engineering 186: 107818 DOI: https://doi.org/10.1016/j.compositesb.2020.107818.

[ANSYS 2015] ANSYS.(2015) "*ANSYS Structural Mechancis*". Pennsylvania, ANSYS Inc.http://www.ansys.com/.

[Arruda et al. 2021] Arruda, M. R. T., Almeida-Fernandes, L., Castro, L. and Correia, J. R.(2021) "*Tsai–Wu based orthotropic damage model*." Composites Part C: Open Access 4: 100122 DOI: https://doi.org/10.1016/j.jcomc.2021.100122.

[Arruda et al. 2018] Arruda, M. R. T., Castro, L. M. S., Ferreira, A. J. M., Martins, D. and Correia, J. R.(2018) "*Physically non-linear analysis of beam models using Carrera Unified Formulation*." Composite Structures 195: 60-73 DOI: https://doi.org/10.1016/j.compstruct.2018.03.107.

[Arruda et al. 2023] Arruda, M. R. T., Trombini, M. and Pagani, A.(2023) "*Implicit to Explicit Algorithm for ABAQUS Standard User-Subroutine UMAT for a 3D Hashin-Based Orthotropic Damage Model*." Applied Sciences 13(2): 1155.

[Arteiro et al. 2019] Arteiro, A., Catalanotti, G., Reinoso, J., Linde, P. and Camanho, P. P.(2019) "*Simulation of the Mechanical Response of Thin-Ply Composites: From Computational Micro-Mechanics to Structural Analysis*." Archives of Computational Methods in Engineering 26(5): 1445-1487 DOI: 10.1007/s11831-018-9291-2.

[Barbero 2013] Barbero, E. J.(2013) "*Finite Element Analysis of Composite Materials using ABAQUS*". London, CRC Press.

[Barbero et al. 2014] Barbero, E. J. and Cosso, F. A.(2014) "*Determination of material parameters for discrete damage mechanics analysis of carbon-epoxy laminates*." Composites Part B: Engineering 56: 638-646 DOI: https://doi.org/10.1016/j.compositesb.2013.08.084.

[Barbero et al. 2013] Barbero, E. J., Cosso, F. A., Roman, R. and Weadon, T. L.(2013) "*Determination of material parameters for Abaqus progressive damage analysis of E-glass epoxy laminates*." Composites Part B: Engineering 46(Supplement C): 211-220 DOI: https://doi.org/10.1016/j.compositesb.2012.09.069.

[Bazant et al. 1983] Bazant, Z. P. and Oh, B. H.(1983) "*Crack band theory for fracture of concrete*." Materials and Structures 16: 155-177.

[Borst et al. 2012] Borst, R., Crisfield, M. A., Remmers, J. J. C. and Verhoosel, C. V.(2012) "*Nonlinear Finite Element Analysis of Solids and Structures*". UK, Wiley.

[Camanho et al. 2015] Camanho, P. P., Arteiro, A., Melro, A. R., Catalanotti, G. and Vogler, M.(2015) "*Three-dimensional invariant-based failure criteria for fibre-reinforced composites*." International Journal of Solids and Structures 55: 92-107 DOI: https://doi.org/10.1016/j.ijsolstr.2014.03.038.

[Camanho et al. 1999] Camanho, P. P. and Matthews, F. L.(1999) "*A Progressive Damage Model for Mechanically Fastened Joints in Composite Laminates*." Journal of Composite Materials 33(24): 2248-2280 DOI: 10.1177/002199839903302402.

[Carol et al. 2002] Carol, I., Rizzi, E. and William, K.(2002) "*An extended volumetric/deviatoric formulation of anisotropic damage based on pseudo-log rate*." European Journal of Mechanics A/Solids 21(5): 747-772.

[Chaboche et al. 2001] Chaboche, J. L., Feyel, F. and Monerie, Y.(2001) "*Interface debonding models; a viscous regularization with a limited rate dependency*." International Journal of Solids and Structures 38: 3127-3160.

[Chell et al. 1976] Chell, G. G. and Worthington, P. J.(1976) "*The determination of fracture toughness of a tough steel from invalid compact tension specimens of varying width and thickness*." Materials Science and Engineering 26(1): 95-103 DOI: https://doi.org/10.1016/0025-5416(76)90231-7.

[Chen et al. 2022] Chen, X., Sun, X., Wang, B., Gu, J., Zou, P., Chai, Y. and Yang, J.(2022) "*An improved longitudinal failure criterion for UD composites based on kinking model*." Mechanics of Advanced Materials and Structures 29(6): 905-915 DOI: 10.1080/15376494.2020.1799269.

[Chen et al. 2019] Chen, Z., Fang, G., Xie, J. and Liang, J.(2019) "*Mechanism-based strength criterion for 3D needled C/C–SiC composites under in-plane biaxial compression*." Mechanics of Advanced Materials and Structures 26(22): 1841-1848 DOI: 10.1080/15376494.2018.1452316.

[Cheng et al. 2017] Cheng, X., Wang, S., Zhang, J., Huang, W., Cheng, Y. and Zhang, J.(2017) "*Effect of damage on failure mode of multi-bolt composite joints using failure envelope method*." Composite Structures 160: 8-15 DOI: https://doi.org/10.1016/j.compstruct.2016.10.042.

[Chowdhury et al. 2021] Chowdhury, U. and Wu, X.-F.(2021) "*Cohesive Zone Modeling of the Elastoplastic and Failure Behavior of Polymer Nanoclay Composites*." Journal of Composites Science 5(5): 131.

[CNR-DT-205/2007 2008] CNR-DT-205/2007.(2008) "*Guide for the Design and Construction of Structures made of FRP Pultruded Elements*". Italy, Advisory Committee on Technical Recommendations for Construction

[Correia et al. 2015] Correia, J. R., Martins, D., Gonilha, J., Arruda, M., Andre, C., Nascimento, J. and Branco, F.(2015)] "*Clickhouse project an all composite emergency housing system*". CACM Conference on Advances in Composite Materials and Structures, Instambul.

[Dhari et al. 2021] Dhari, R. S., Patel, N. P., Wang, H. and Hazell, P. J.(2021) "*Progressive damage modeling and optimization of fibrous composites under ballistic impact loading*." Mechanics of Advanced Materials and Structures 28(12): 1227-1244 DOI: 10.1080/15376494.2019.1655688.

[Dunne et al. 2005] Dunne, F. and Petrinic, N.(2005) "*Introduction to Computational Plasticity*". New York, 1, Oxford University Press.

[Duvaut et al. 1972] Duvaut, G. and Lions, J. L.(1972) "*Les Inequations en Mecanique et en Physique*". Paris, Dunod.

[El Kadi et al. 2022] El Kadi, M., Van Hemelrijck, D. and Tysmans, T.(2022) "*Improving the Anchorage in Textile Reinforced Cement Composites by 3D Spacer Connections: Experimental Study of Flexural and Cracking Behaviors*." Journal of Composites Science 6(12): 357.

[Forero et al. 2021] Forero, J. A., Bravo, M., Pacheco, J., de Brito, J. and Evangelista, L.(2021) "*Fracture Behaviour of Concrete with Reactive Magnesium Oxide as Alternative Binder*." Applied Sciences 11(7): 2891.

[Geers et al. 1994] Geers, M. G. D., Brekelmans, W. A. M. and de Borst, R.(1994)] "*Viscous Regularization of Strain-Localisation for Damaging Materials*", Dordrecht, Springer Netherlands.

[Girão Coelho et al. 2015] Girão Coelho, A. M., Toby Mottram, J. and Harries, K. A.(2015) "*Finite element guidelines for simulation of fibre-tension dominated failures in composite materials validated by case studies*." Composite Structures 126: 299-313 DOI: https://doi.org/10.1016/j.compstruct.2015.02.071.

[Granados et al. 2021] Granados, J. J., Martinez, X., Nash, N., Bachour, C., Manolakis, I., Comer, A. and Di Capua, D.(2021) "*Numerical and experimental procedure for material calibration using the serial/parallel mixing theory, to analyze different composite failure modes*." Mechanics of Advanced Materials and Structures 28(14): 1415-1433 DOI: 10.1080/15376494.2019.1675106.

[Gutkin et al. 2009] Gutkin, R. and Pinho, S. T.(2009) "*PRACTICAL APPLICATION OF FAILURE MODELS TO PREDICT THE RESPONSE OF COMPOSITE STRUCTURES*". 18TH INTERNATIONAL CONFERENCE ON COMPOSITE MATERIALS. Lisbon-Portugal.

[Hashin 1980] Hashin, Z.(1980) "*Failure Criteria for Unidirectional Fiber Composites*." Journal of Applied Mechanics 47(2): 329-334 DOI: 10.1115/1.3153664.

[Hashin 1981] Hashin, Z.(1981) "*Fatigue Failure Criteria for Unidirectional Fiber Composites*." Journal of Applied Mechanics 48(4): 846-852 DOI: 10.1115/1.3157744.

[Hashin et al. 1973] Hashin, Z. and Rotem, A.(1973) "*A Fatigue Failure Criterion for Fiber Reinforced Materials*." Journal of Composite Materials 7(4): 448-464 DOI: 10.1177/002199837300700404.

[Hu et al. 2022] Hu, H., Wei, Q., Liu, B., Liu, Y., Hu, N., Ma, Q. and Wang, C.(2022) "*Progressive Damage Behaviour Analysis and Comparison with 2D/3D Hashin Failure Models on Carbon Fibre–Reinforced Aluminium Laminates*." Polymers 14(14): 2946.

[Hühne et al. 2010] Hühne, C., Zerbst, A. K., Kuhlmann, G., Steenbock, C. and Rolfes, R.(2010) "*Progressive damage analysis of composite bolted joints with liquid shim layers using constant and continuous degradation models*." Composite Structures 92(2): 189-200 DOI: https://doi.org/10.1016/j.compstruct.2009.05.011.

[Kaddour et al. 2013] Kaddour, A. and Hinton, M.(2013) "*Maturity of 3D failure criteria for fibre-reinforced composites: Comparison between theories and experiments: Part B of WWFE-II*." Journal of Composite Materials 47(6-7): 925-966 DOI: 10.1177/0021998313478710.

[Kang et al. 2021] Kang, I.-K. and Kim, S.-H.(2021) "*Compressive Strength Testing of Hybrid Concrete-Filled Fiber-Reinforced Plastic Tubes Confined by Filament Winding*." Applied Sciences 11(7): 2900.

[Kong et al. 2020] Kong, S. Y., Wong, L. S., Paul, S. C. and Miah, M. J.(2020) "*Shear Response of Glass Fibre Reinforced Polymer (GFRP) Built-Up Hollow and Lightweight Concrete Filled Beams: An Experimental and Numerical Study*." Polymers 12(10): 2270.

[Lapczyk et al. 2007] Lapczyk, I. and Hurtado, J. A.(2007) "*Progressive damage modeling in fiber-reinforced materials*." Composites Part A: Applied Science and Manufacturing 38(11): 2333-2341 DOI: https://doi.org/10.1016/j.compositesa.2007.01.017.

[Lemaitre 1992] Lemaitre, J.(1992) "*A Course on Damage Mechanics*". Verlag, Springer.

[Lemaitre et al. 2002] Lemaitre, J., Benallal, A., Billardon, R. and Marquis, D.(2002) "*Thermodynamics and phenomenology*." In Continuum Thermomechanics - The Art and Science of Modelling Material Behaviour, Solid Mechanics and Its Applications 76: 209-223 Springer Netherlands.

[Lemaitre et al. 2005] Lemaitre, J. and Desmorat, R.(2005) "*Engineering Damage Mechanics*". Berlin Heidelberg, Springer.

[Li et al. 2021] Li, B., Gong, Y., Xiao, H., Gao, Y. and Liang, E.(2021) "*A Two-Dimensional Model for Pin-Load Distribution and Failure Analysis of Composite Bolted Joints*." Materials 14(13): 3646.

[Li et al. 2017] Li, S., Sitnikova, E., Liang, Y. and Kaddour, A.-S.(2017) "*The Tsai-Wu failure criterion rationalised in the context of UD composites*." Composites Part A: Applied Science and Manufacturing 102: 207-217 DOI: https://doi.org/10.1016/j.compositesa.2017.08.007.

[Linde et al. 2004] Linde, P., Pleitner, J., Boer, H. and Carmone, C.(2004) "*Modelling and Simulation of Fibre Metal Laminates*". 2004 ABAQUS Users' Conference. Boston Massachusetts.

[Liu et al. 2020] Liu, H., Liu, J., Ding, Y., Zhou, J., Kong, X., Harper, L. T., Blackman, B. R. K., Falzon, B. G. and Dear, J. P.(2020) "*Modelling damage in fibre-reinforced thermoplastic composite laminates subjected to three-point bend loading*." Composite Structures 236: 111889 DOI: https://doi.org/10.1016/j.compstruct.2020.111889.

[Liu et al. 2014] Liu, Y., Zwingmann, B. and Schlaich, M.(2014) "*Nonlinear Progressive Damage Analysis of Notched or Bolted Fibre-Reinforced Polymer (FRP) Laminates Based on a Three-Dimensional Strain Failure Criterion*." Polymers 6(4): 949.

[Lopes et al. 2020] Lopes, B., Arruda, M. R. T., Almeida-Fernandes, L., Castro, L., Silvestre, N. and Correia, J. R.(2020) "*Assessment of mesh dependency in the numerical simulation of compact tension tests for orthotropic materials*." Composites Part C: Open Access 1: 100006 DOI: https://doi.org/10.1016/j.jcomc.2020.100006.

[Mandal et al. 2017] Mandal, B. and Chakrabarti, A.(2017) "*Simulating Progressive Damage of Notched Composite Laminates with Various Lamination Schemes*." International Journal of Applied Mechanics and Engineering 22(2): 333-347 DOI: doi:10.1515/ijame-2017-0020.

[Martinavičius et al. 2020] Martinavičius, D., Augonis, M. and Rui Tiago Arruda, M.(2020) "*Experimental and Analytical Study on Local Buckling Behavior of the Concrete-filled Thin-walled Welded Steel Columns*." Periodica Polytechnica Civil Engineering 64(3): 917-927 DOI: 10.3311/PPci.15705.

[Martins et al. 2021] Martins, D., Gonilha, J., Correia, J. R. and Silvestre, N.(2021) "*Exterior beam-to-column bolted connections between GFRP I-shaped pultruded profiles using stainless steel cleats. Part 1: Experimental study*." Thin-Walled Structures 163: 107719 DOI: https://doi.org/10.1016/j.tws.2021.107719.

[Martins et al. 2017] Martins, D., Proença, M., Correia, J. R., Gonilha, J., Arruda, M. and Silvestre, N.(2017) "*Development of a novel beam-to-column connection system for pultruded GFRP tubular profiles*." Composite Structures 171: 263-276 DOI: https://doi.org/10.1016/j.compstruct.2017.03.049.

[Matzenmiller et al. 1995] Matzenmiller, A., Lubliner, J. and Taylor, R. L.(1995) "*A constitutive model for anisotropic damage in fiber-composites*." Mechanics of Materials 20(2): 125-152 DOI: http://dx.doi.org/10.1016/0167-6636(94)00053-0.

[Melro 2011] Melro, A. R.(2011) "*Analytical and Numerical Modelling of Damage and Fracture of Advanced Composites*". Department of Mechanical Engineering. Portugal, FEUP. *Phd*.

[Naderi et al. 2013] Naderi, M. and Khonsari, M. M.(2013) "*Stochastic analysis of inter- and intra-laminar damage in notched PEEK laminates*." Express Polymer Letters 7: 383-395 DOI: 10.3144/expresspolymlett.2013.35.

[Nahas 1986] Nahas, M.(1986) "*SURVEY OF FAILURE AND POST-FAILURE THEORIES OF LAMINATED FIBER-REINFORCED COMPOSITES*." Journal of Composites Technology and Research 8: 138-153.

[Nguyen 1985] Nguyen, Q. S.(1985) "*Uniqueness, stability and bifurcation of standard systems*". Current Trends and Results in Plasticity. London, Elsevier.

[Oliver 1989] Oliver, J.(1989) "*A consistent characteristic length for smeared cracking models*." International Journal for Numerical Methods in Engineering 28: 461-474.

[Olmedo et al. 2012] Olmedo, Á. and Santiuste, C.(2012) "*On the prediction of bolted single-lap composite joints*." Composite Structures 94(6): 2110-2117 DOI: https://doi.org/10.1016/j.compstruct.2012.01.016.

[Proença 2000] Proença, S. P. B.(2000) "*Introdução à mecânica do dano e fracturamento, Notas de aulas*". Escola de Engenharia de São Carlos, Universidade de São Carlos, São Paulo.

[Rahimian Koloor et al. 2020] Rahimian Koloor, S. S., Karimzadeh, A., Yidris, N., Petrů, M., Ayatollahi, M. R. and Tamin, M. N.(2020) "*An Energy-Based Concept for Yielding of Multidirectional FRP Composite Structures Using a Mesoscale Lamina Damage Model*." Polymers 12(1): 157.

[Srinivasa et al. 2022] Srinivasa, A. R., Reddy, J. N. and Phan, N.(2022) "*A discrete nonlocal damage mechanics approach*." Mechanics of Advanced Materials and Structures 29(13): 1813-1820 DOI: 10.1080/15376494.2020.1839984.

[Tsai 1984] Tsai, S. W.(1984) "*A Survey of Macroscopic Failure Criteria for Composite Materials*." Journal of Reinforced Plastics and Composites 3(1): 40-62 DOI: 10.1177/073168448400300102.

[Tsai et al. 1980] Tsai, S. W. and Hahn, H. T.(1980) "*Introduction to composite materials*". Westport, Conn., Technomic Pub.

[Tsai et al. 1971] Tsai, S. W. and Wu, E. M.(1971) "*A General Theory of Strength for Anisotropic Materials*." Journal of Composite Materials 5(1): 58-80 DOI: 10.1177/002199837100500106.

[Wang et al. 2017] Wang, C., Roy, A., Silberschmidt, V. V. and Chen, Z.(2017) "*Modelling of Damage Evolution in Braided Composites: Recent Developments*." Mechanics of Advanced Materials and Modern Processes 3(1): 15 DOI: 10.1186/s40759-017-0030-4.

[Wang et al. 2018] Wang, G.-D. and Melly, S. K.(2018) "*Three-dimensional finite element modeling of drilling CFRP composites using Abaqus/CAE: a review*." The International Journal of Advanced Manufacturing Technology 94(1): 599-614 DOI: 10.1007/s00170-017-0754-7.

[Wang et al. 2009] Wang, Y., Tong, M. and Zhu, S.(2009)] "*Three Dimensional Continuum Damage Mechanics Model of Progressive Failure Analysis in Fibre-Reinforced Composite Laminates*". Structures, Structural Dynamics, and Materials Conference, California.

[Warren et al. 2016] Warren, K. C., Lopez-Anido, R. A., Vel, S. S. and Bayraktar, H. H.(2016) "*Progressive failure analysis of three-dimensional woven carbon composites in single-bolt, double-shear bearing*." Composites Part B: Engineering 84: 266-276 DOI: http://dx.doi.org/10.1016/j.compositesb.2015.08.082.

[Xiong et al. 2022] Xiong, Z., Zhao, C., Meng, Y. and Li, W.(2022) "*A damage model based on Tsai–Wu criterion and size effect investigation of pultruded GFRP*." Mechanics of Advanced Materials and Structures: 1-15 DOI: 10.1080/15376494.2022.2116754.

[Zhan et al. 2023] Zhan, P., Qin, X., Zhang, Q. and Sun, Y.(2023) "*Damage identification in beam-like structure using strain FRF-based damage index and artificial neural network*." Mechanics of Advanced Materials and Structures 30(12): 2458-2476 DOI: 10.1080/15376494.2022.2055241.

[Zhuang et al. 2019] Zhuang, F., Arteiro, A., Furtado, C., Chen, P. and Camanho, P. P.(2019) "*Mesoscale modelling of damage in single- and double-shear composite bolted joints*." Composite Structures 226: 111210 DOI: https://doi.org/10.1016/j.compstruct.2019.111210.

[Ziegler 1977] Ziegler, H.(1977) "*An introduction to thermomechanics*". North-Holland.